outcome. The presence of CCD in the subacute stage may be useful in diagnosing the location and extension of the cerebral ischemic lesion involved in the cerebropontocerebellar pathway (19, 22). However, to our knowledge, no reports about the prognostic clinical value of CCD regarding the outcome of stroke in the subacute stage have been published. These findings have shown that CCD in the early subacute stage after MCA territory infarction with hemispheric symptoms is correlated with neurologic severity and the degree of disability 60 days after the onset of symptoms. The negative direction of these correlations means that, as the degree of cerebellar hypoperfusion in the subacute stage increases, the neurologic outcome worsens.

Serrati et al (5) used the Mathew and Orgogozo scales to study the relationship between crossed cerebellar hypometabolism and clinical outcome on day 60. They reported that crossed cerebellar hypometabolism in the early chronic stage is strongly associated with neurologic outcome, as measured with cerebellar oxygen consumption. In a retrospective study, De Reuck et al (6) reported that PET findings and Orgogozo scores indicated better neurologic improvement in patients without significant CCD in the late chronic stage (4–24 months) of MCA infarcts than that of other patients. We performed SPECT at an earlier stage (ie, early subacute stage); to our knowledge, examination at this stage has not been studied. Cerebellar hypoperfusion in the subacute stage may persist in the chronic stage; therefore, the degree of cerebellar hypoperfusion in the subacute stage may be associated with clinical outcome.

Conclusion

The significant correlation between cerebellar hypoperfusion in the early subacute stage and clinical outcome at 60 days was revealed in this study. This finding suggests that CCD in the early subacute stage may be a valuable prognostic factor in patients with stroke.

Acknowledgments

We thank Shigeru Yoneda and Hiroshi Nakao of the Department of Radiology for technical support in performing brain SPECT imaging.

References

1. Baron JC, Bousser MG, Comar D, Castaigne P. **Crossed cerebellar diaschisis in human supratentorial brain infarction.** *Trans Am Neurol Assoc* 1980;105:459–461
2. Lenzi GL, Frackowiak RS, Jones T. **Cerebral oxygen metabolism and blood flow in human cerebral ischemic infarction.** *J Cereb Blood Flow Metab* 1982;2;321–335
3. Kushner M, Alavi A, Reivich M, Dann R, Burke A, Robinson G. **Contralateral cerebellar hypometabolism following cerebral insult: a positron emission tomographic study.** *Ann Neurol* 1984;15:425–434
4. Pantano P, Baron JC, Samson Y, Bousser MG, Derouesne C, Comar D. **Crossed cerebellar diaschisis: further studies.** *Brain* 1986;109:677–694
5. Serrati C, Marchal G, Rioux P, et al. **Contralateral cerebellar hypometabolism: a predictor for stroke outcome.** *J Neurol Neurosurg Psychiatry* 1994;57:174–179
6. De Reuck J, Decoo D, Lemahieu I, Strijckmans K, Goethals P, Maele GV. **Crossed cerebellar diaschisis after cerebral artery infarction.** *Clin Neurology Neurosurg* 1997;99:11–16
7. Infeld B, Davis SM, Lichtenstein M, Mitchell PJ, Hopper JL. **Crossed cerebellar diaschisis and brain recovery after stroke.** *Stroke* 1995;26:90–95
8. Laloux P, Richelle F, Jamart J, Coster PD, Laterre C. **Comparative correlations of HMPAO SPECT indices, neurological score, and stroke subtypes with clinical outcome in acute carotid infarcts.** *Stroke* 1995;26:816–821
9. Adams HP, Brott TG, Furlan AJ, et al. **Guidelines for thrombolytic therapy for acute stroke: a supplement to the guidelines for the management of patients with acute ischemic stroke: a statement for healthcare professionals from a special writing group of the Stroke Council, American Heart Association.** *Stroke* 1996;27:1711–1718
10. Kuwabara Y, Ichiyama Y, Sasaki M, et al. **Cerebellar vascular response to acetazolamide in crossed cerebellar diaschisis: a comparison of 99mTc-HMPAO single-photon emission tomography with 15O-H2O positron emission tomography.** *Eur J Nucl Med* 1996;23:683–689
11. Scandinavian Stroke Study Group. **Multicenter trial of hemodilution in ischemic stroke.** *Stroke* 1985;16:885–890
12. Granger CV, Hamilton BB, Gresham GE, Kramer AA. **The stroke rehabilitation outcome study, II: relative merits of the total Barthel Index score and a four-item subscore in predicting patient outcome.** *Arch Phys Med Rehabil* 1989;70:100–103
13. Shah S, Vanclay F, Cooper B. **Efficiency, effectiveness, and duration of stroke rehabilitation.** *Stroke* 1990;21:241–246
14. Kim SE, Choi CW, Yoon BW, et al. **Crossed-cerebellar diaschisis in cerebral infarction: Technetium-99m-HMPAO SPECT and MRI.** *J Nucl Med* 1997;38:14–19
15. Kushner M, Kaasik AE, Nencini P, et al. **Contralateral cerebellar hypometabolism following cerebral infarction: an acute and follow-up study.** *Neurology* 1988;38:147
16. Yamauchi H, Fukuyama H, Yamaguchi S, et al. **Crossed cerebellar hypoperfusion in unilateral major cerebral artery occlusive disorders.** *J Nucl Med* 1992;33:1632–1636
17. Reivich M. **Crossed cerebellar diaschisis.** *AJNR Am J Neuroradiol* 1992;13:62–64
18. Heiss WD. **Experimental evidence of ischemic thresholds and functional recovery.** *Stroke* 1992;23:1668–1672
19. Moretti JL, Defer G, Cinotti L, et al. **"Luxury perfusion" with Tc-99m HMPAO and I-123 IMP SPECT imaging during the subacute phase of stroke.** *Eur J Nucl Med* 1990;16:17–22
20. Sperling B, Lassen NA. **Hyperfixation of HMPAO in subacute ischemic stroke leading to spuriously high estimates of cerebral blood flow by SPECT.** *Stroke* 1993;24:193–194
21. Bowler JV, Wade JPH, Jones BE, Nijran KS, Steiner TJ. **Natural history of the spontaneous reperfusion of human cerebral infarcts as assessed by 99mTc HMPAO SPECT.** *J Neurol Neurosurg Psychiatry* 1998;64:90–97
22. Lin WY, Kao CH, Wang PY, Changlai SP, Wang SJ. **Serial changes in regional blood flow in the cerebrum and cerebellum of stroke patients imaged by 99mTc-HMPAO SPECT.** *Nucl Med Commun* 1996;17:208–211

Detection of Misery Perfusion With Split-Dose ^{123}I-Iodoamphetamine Single-Photon Emission Computed Tomography in Patients With Carotid Occlusive Diseases

Masao Imaizumi, MD; Kazuo Kitagawa, MD, PhD; Kazuo Hashikawa, MD, PhD; Naohiko Oku, MD, PhD; Tadamasa Teratani, MD; Masashi Takasawa, MD; Takuya Yoshikawa, MD; Piao Rishu, MD; Toshiho Ohtsuki, MD, PhD; Masatsugu Hori, MD, PhD; Masayasu Matsumoto, MD, PhD; Tsunehiko Nishimura, MD, PhD

Background and Purpose—Patients with carotid occlusive disease and stage 2 cerebral hemodynamic failure, characterized by an increased oxygen extraction fraction (OEF) as measured by positron emission tomography (PET) and otherwise known as misery perfusion, have a high risk of cerebral ischemia and subsequent stroke. In clinical practice, the detection of patients with misery perfusion through the use of widely available, noninvasive, and cost-effective modalities such as single-photon emission computed tomography (SPECT) is extremely important.

Methods—We evaluated the relationships between the regional hemodynamic status of cerebral circulation, measured with split-dose [^{123}I] *N*-isopropyl-p-iodoamphetamine SPECT (^{123}I-IMP SPECT) and an acetazolamide challenge, and hemodynamic parameters, including OEF measured with PET, in 27 patients with both unilateral and bilateral carotid occlusive diseases.

Results—A significant negative correlation was found between the SPECT-measured cerebrovascular reserve after acetazolamide administration and both the PET-measured OEF and cerebral blood volume. Neither the cerebrovascular reserve nor the cerebral blood flow index, when expressed as a SPECT-measured cerebrum-to-cerebellum ratio, was useful for detecting lesions with an elevated OEF. However, a combination of the cerebrovascular reserve and cerebral blood flow index showed high sensitivity, specificity, and positive predictive value for the detection of misery perfusion.

Conclusions—Our study suggests that split-dose ^{123}I-IMP SPECT with an acetazolamide challenge could be useful for screening patients with misery perfusion in carotid occlusive diseases. (***Stroke.* 2002;33:2217-2223.)

Key Words: acetazolamide ■ hemodynamics ■ tomography, emission computed

Severe atherosclerotic disease of the carotid and vertebral arteries or their intracranial branches may cause hemodynamic impairment of the distal cerebral circulation. Several studies have shown that patients with hemodynamics have a high risk of subsequent ischemic stroke[1–3]; therefore, the identification and treatment of high-risk patients could help to prevent stroke. Among the various methods of hemodynamic assessment, positron emission tomography (PET) is the most reliable tool for the quantitative assessment of blood supply and metabolic demand. When PET with ^{15}O gases is used, the hemodynamic effect can be categorized into 3 stages: stage 0, normal cerebral hemodynamics; stage 1, autoregulatory vasodilatation in which the cerebral blood volume (CBV) is increased and other parameters are normal; and stage 2, in which the cerebral blood flow (CBF) is reduced and the oxygen extraction fraction (OEF) is increased to maintain the cerebral metabolic rate of oxygen ($CMRO_2$) and CBV.[4] Stage 2 has been called "misery perfusion" and represents an inadequate blood supply relative to metabolic demand.[5] The presence of an increased OEF lesion can be a predictor of subsequent ischemic stroke.[2,3] In clinical practice, the detection of misery perfusion in patients with carotid occlusive disease is important for the prevention of stroke and may be performed with widely available, noninvasive, and cost-effective modalities such as single-photon emission computed tomography (SPECT). However, the conventional method of measuring cerebrovascular reserve (CVR) with SPECT takes >2 days to perform and requires arterial blood sampling. We have developed a split-dose [^{123}I] *N*-isopropyl-p-iodoamphetamine (^{123}I-IMP) SPECT method, followed by an acetazolamide (ACZ) challenge, that enables noninvasive and semiquantitative measurements of regional CBF and CVR to be performed in 1 hour.[6,7] Although several studies have shown a relationship between impaired CVR measured

Received March 18, 2002; final revision received May 3, 2002; accepted May 7, 2002.

From the Division of Tracer Kinetics (M.I., N.O., T.T., P.R., T.N.) the Department of Internal Medicine and Therapeutics (K.K., K.H., M.T., T.Y., T.O., M.H., M.M.), Osaka University Graduate School of Medicine, Suita, Osaka, Japan.

Correspondence to Masao Imaizumi, MD, Division of Tracer Kinetics, Osaka University Graduate School of Medicine, 2-2, Yamadaoka, Suita City, Osaka, 565-0871, Japan. E-mail imaizumi@tracer.med.osaka-u.ac.jp

Stroke is available at http://www.strokeaha.org

DOI: 10.1161/01.STR.0000027638.19392.7E

Patient Characteristics

Patient	Age, y	Sex	Neurological Deficits	Disease	Angiographical Findings	MRI Findings
1	72	M	None	Asymptomatic	R ICAS	R BG
2	69	F	L sensory disturbance	CI	R MCAO	R BG~CR
3	70	F	Dysarthria	CI	L ICAO	L BG~CR
4	65	M	None	Asymptomatic	R ICAS	None
5	73	F	Visual field defect	CI	L ICAS	R temporal~occipital subcortex
6	59	M	L sensory disturbance	TIA	R MCAS, & L ICAS	Bil BG~deep white matter
7	67	M	Syncope	CI	R ICAO	Bil BG
8	62	M	R sensory disturbance	CI	L MCAS	L BG
9	61	M	Dizziness	CI	Bil ICAS	Bil deep white matter
10	75	F	Dizziness	CI	L MCAS	L CR
11	61	F	R hemiparesis	TIA	L ICAO	None
12	63	F	None	Asymptomatic	L ICAS	None
13	28	F	L hemiparesis	TIA	Bil MCAS	None
14	31	F	R hemiparesis	CI	Bil ICAS	R BG
15	60	M	Perseveration	CI	L MCAS	L BG
16	67	M	Dizziness	Asymptomatic	L ICAO	L BG, L frontoparietal subcortex
17	54	M	Visual field defect	CI	R MCAS	R BG
18	63	F	None	Asymptomatic	L ICAS	Bil BG~CR
19	68	M	R hemiparesis	TIA	L MCAS	Pons
20	66	M	R hemiparesis	CI	L MCAO, R ICAS	Bil BG
21	64	F	L hemiparesis	CI	R ICAO	R frontal lobe
22	70	M	R hemiparesis	CI	R ICAO	L BG
23	35	M	L hemiparesis	TIA	R ICAO	None
24	63	F	R hemiparesis & motor aphasia	CI	L ICAS	L BG~CR
25	69	F	L hemiparesis	TIA	R ICAO	None
26	54	F	Motor aphasia	CI	L MCAO	L CR
27	71	M	L hemiparesis	TIA	R ICAO	R temporal, parietooccipital subcortex

Asymptomatic indicates asymptomatic carotid artery disease; ICAS, internal carotid artery stenosis; BG, basal ganglia; CI, cerebral infarction; MCAO, MCA occlusion; CR, corona radiata; ICAO, internal carotid artery occlusion; TIA, transient ischemic attack; MCAS, MCA stenosis; and Bil, bilateral.

by ACZ injection or CO_2 inhalation with SPECT and an increased OEF measured by PET,[8–11] it remains unsettled as to whether an ACZ challenge and split-dose ^{123}I-IMP SPECT can be used to detect patients with misery perfusion. Therefore, the purpose of this study was to clarify the relationship between the CVR and CBF index measured by routine split-dose ^{123}I-IMP SPECT and the hemodynamic parameters measured by PET in 27 carotid occlusive diseases.

Subjects and Methods

Enrollment in this study began on February 16, 2000, and ended on July 10, 2001. A total of 43 consecutive patients with chronic cerebrovascular diseases were examined with both SPECT and PET during this period at the Osaka University Medical School Hospital. Before the SPECT and PET examinations, each subject underwent neurological and neuroradiological evaluations, including an evaluation for occlusive cerebrovascular disease by duplex carotid ultrasonography, MRI, MR angiography (MRA), and cerebral angiography. The MRI examination was performed in 5-mm-thick sections along the orbitomeatal plane with a 1.5-T unit. Infarction was defined as a focal area with prolonged T1 and T2 relaxation times. The interval between the MRI study and the SPECT and PET studies was <30 days. The SPECT study was performed at least 4 weeks after the patient's most recent clinical episode, once the neurological condition had stabilized. Two neuroradiologists who were unaware of the patients' medical histories and diagnoses independently reviewed the MRI, SPECT, and PET images. A cerebral angiography was performed in all patients. The maximum percentage of stenosis and the presence of ulceration were evaluated according to the recommendations of the North American Symptomatic Carotid Endarterectomy Trial.[12]

The mechanism of stroke was clinically diagnosed in each patient and classified according to the National Institute of Neurological Disorders and Stroke classification of cerebrovascular disease III.[13] Patients with cardioembolic infarctions were excluded from the study. Finally, we selected 27 consecutive patients (13 men, 14 women; mean±SD age, 61.5±12.1 years) with occlusion or stenosis of the internal carotid artery or the main trunk of the middle cerebral artery (MCA) to be included in this study. Fifteen patients had a small cerebral infarction (<15 mm in diameter), 7 had transient ischemic attacks, and 5 had asymptomatic carotid artery disease. The clinical feature, angiographic findings, and MRI findings are summarized in the Table.

SPECT Imaging

We used a high-performance, 4-head rotating gamma camera equipped with a low-energy, general-purpose, parallel-hole collimator with a spatial resolution of 13.0-mm full width at half-maximum (Gamma View SPECT 2000H, Hitachi Medical Co). Data were acquired in a continuous rotating mode in reciprocal directions at 20 seconds per revolution for 66 minutes from 96 directions in a 64×64 matrix. The transaxial images were reconstructed with a Butterworth

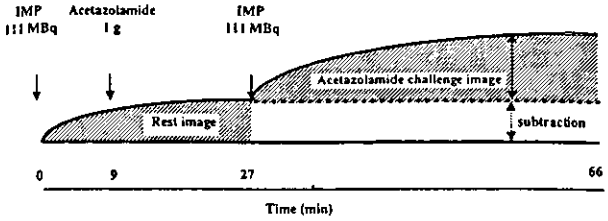

Figure 1. Split-dose IMP-SPECT (dynamic imaging protocol). During an ~1-hour SPECT acquisition, double injections of 111 MBq ^{123}I-IMP were performed before and after ACZ administration. Two perfusion images (resting and ACZ challenge) were obtained with the subtraction technique.

filter. During the dynamic SPECT, 111 MBq ^{123}I-IMP (Nihon Mediphysics) was intravenously injected at the start of imaging, and 1 g ACZ (Diamox, Lederle Ltd) was slowly injected intravenously over a 1-minute period 9 minutes after the initial ^{123}I-IMP injection. An additional 111 MBq ^{123}I-IMP was injected 27 minutes after the start of imaging. Two perfusion images, resting and vasodilated, were obtained with the subtraction technique (Figure 1).

PET Imaging

All patients were scanned with a Headtome V/SET 2400W system (Shimadzu Co, Ltd), which acquires 63 slices with an interslice distance of 3.1 mm. All scans were performed at a resolution of 3.7-mm full width at half-maximum in the transaxial direction and at 5 mm in the axial direction. The patient's head was fixed in place with a head holder and was positioned with light beams to obtain transaxial slices parallel to the orbitomeatal line. Before the PET study, germanium-68–gallium-68 transmission scanning was performed for 10 minutes for attenuation correction. Images were reconstructed with an ordered-subset expectation maximization algorithm (12 iterations with 4 ordered subsets). For the ^{15}O-labeled gas steady-state method, $C^{15}O_2$ (550 MBq/min) and $^{15}O_2$ (1300 MBq/min) were inhaled through a mask. The scan time was 9 minutes, and arterial blood was manually sampled from the radial artery 4 times during each scan. The concentration of the radiotracer activity in the whole blood and plasma was measured with a well counter; the arterial blood hematocrit, hemoglobin concentration, Pa_{O_2}, and Pa_{CO_2} were also measured. Inhalation of 2000 MBq $C^{15}O$ and a 9-minute scanning period were used to measure the CBV. Arterial sampling was manually performed 3 times during the scanning, and the radiotracer activity in whole blood was measured. CBF, CMR_{O_2}, and OEF were calculated from the steady-state method, and CMR_{O_2} and OEF were corrected according to the CBV. The study protocol was in accordance with the standard ethics guidelines of Osaka University Medical School, and written, informed consent was obtained from all subjects.

Data Analysis

All SPECT and PET data were analyzed with the Dr. View pro5.0 image analysis software system (Asahi Kasei Joho System Co, Ltd) running on a UNIX system and an Indigo 2 station (Silicon Graphics). The region-of-interest (ROI) analysis in this study is illustrated in Figure 2. Circular ROIs, 20 mm in diameter, were placed over the cortex at the levels of the basal ganglia (lower MCA territory), parietal lobe (upper MCA territory), and cerebellar hemispheres in the SPECT and PET images of each patient. To match the slice thickness, the ROIs in each level of the MCA territories were placed over 3 slices (12 mm) on the SPECT images and over 4 slices (12.5 mm) on the PET images. Finally, 108 regions were investigated in 27 patients (4 regions in each patient: right and left, and upper and lower MCA). In the SPECT study, all ROIs generated in the resting image were transferred to the ACZ-challenge image. In the PET study, all of the ROIs generated in the CBF images were transferred to the OEF, CMR_{O_2}, and CBV images. The following equation was used to estimate the percentage increase in regional CBF induced by the ACZ challenge in the form of the CVR: CVR equals ACZ challenge SPECT count minus resting SPECT count divided by resting SPECT count. To estimate the resting CBF, the cerebral cortical ROI counts were normalized to those of the cerebellar hemisphere by use of the higher counts, which eliminated any effects of crossed cerebellar diaschisis.

Seven age-matched patients who complained of nonfocal neurological symptom (dizziness or headache) and who showed no ischemic lesions after MRI and no stenotic lesions in their major cerebral arteries after MRA underwent SPECT examination to determine their control values. The normal control values for CVR and cerebrum-to-cerebellum ratio (CBF index) for the MCA territories made a normal distribution; they were 0.69 ± 0.23 and 0.83 ± 0.09, respectively. The mean CVR after ACZ challenge in the normal subjects was 0.69 in our study, which agrees with previous reports.[14,15] The CBF index and CVR values were judged to be abnormal when they were beyond the range of the mean±2 SD range of the normal control subjects. The 108 MCA territories examined were divided into 2 groups according to the angiographic findings. Group A consisted of MCA areas with a severe stenotic lesion (>70%) in the ipsilateral internal carotid artery system, whereas group NA consisted of those with less or no stenotic lesion. All regions were also classified into 2 groups according to their SPECT CVR values: a reduced CVR group with a CVR of <0.23 (mean−2 SD) and a normal CVR group with a CVR of ≥0.23. Because normal values obtained from healthy control subjects were not available, we used PET parameter values obtained from 7 patients with no infarction and no severe stenosis or occlusion (<50%) who were suffering from nonspecific brain symptoms without focal signs (ie, preoperation for cerebral aneurysm, headache, dizziness, and syncope) as the normal values: CBF, 46.9 ± 11.3 mL · 100 g^{-1} · min^{-1} (mean±SD); OEF, 44.1 ± 4.62%; CMR_{O_2}, 3.39 ± 0.82 mL · 100 g^{-1} · min^{-1}; and CBV, 4.22 ± 0.75%. All regions were classified into 3 groups on the basis of their OEF values: normal group, OEF <48.7% (mean+1 SD of the mean OEF value); slightly increased OEF group, 48.7%≤OEF<53.3% (mean+2 SD of the mean OEF value); and an increased OEF group, OEF ≥53.3%. The increased OEF value was compatible with that beyond the upper 95% confidence limits defined in healthy volunteers.[3] We assessed the relationship between the SPECT and PET parameters in the MCA territories using linear

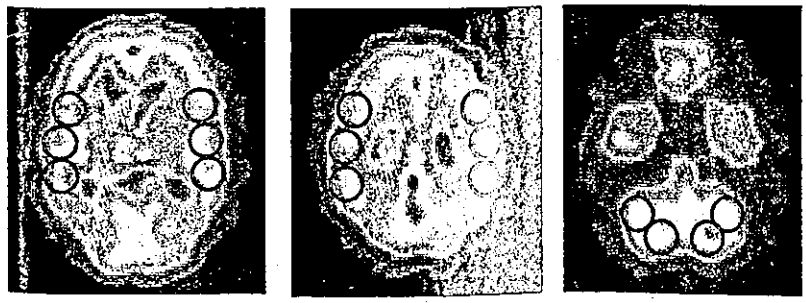

Figure 2. ROI settings. Circular ROIs, 20 mm in diameter, were placed over the cortex at the levels of the basal ganglia (lower MCA territory), parietal lobe (upper MCA territory), and cerebellum in the SPECT and PET images of each patient.

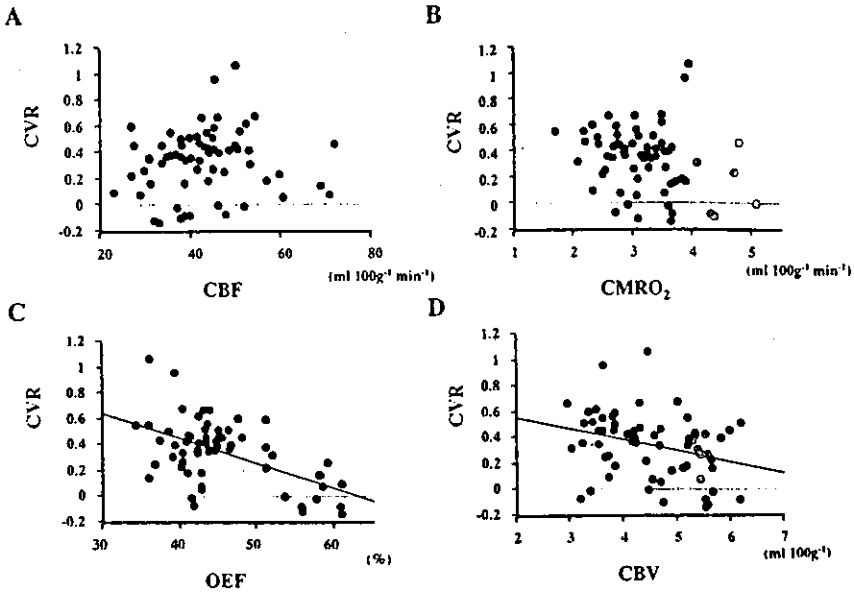

Figure 3. Relationship between CVR and PET parameters on the affected side (group A). A, CBF; B, $CMRo_2$; C, OEF; D, CBV. We compared CVR and PET parameters in group A (n=64). A significant negative correlation was observed between CVR and OEF (C, $r=-0.549$, $P<0.0001$) and between CVR and CBV (D, $r=-0.313$, $P<0.0117$). CBF (A) and $CMRo_2$ (B) were not correlated with the CVR.

regression analysis and Pearson's correlation coefficient. All data are expressed as mean±SD. Differences in data between groups were statistically evaluated with an unpaired t test. Differences with values of $P<0.05$ were considered to be statistically significant.

Results

Comparison of SPECT and PET Parameters

Of the 108 ROIs in all MCA territories, 64 ROIs were on an affected side (group A), and 44 ROIs were on a nonaffected side (group NA), because 5 patients with bilateral carotid disease were included. We compared the CVR and PET parameters in group A and found a significant negative correlation between CVR and OEF ($r=-0.549$, $P<0.0001$; Figure 3) and between CVR and CBV ($r=-0.313$, $P<0.0117$; Figure 3). CBF and $CMRo_2$ were not correlated with the CVR (Figure 3).

Detection of Stage 2 Cerebral Hemodynamic Failure With Semiquantitative SPECT Analysis in Group A

Figure 4 shows the typical MRI, MRA, SPECT, and PET images of a stage 2 patient. The areas of increased OEF and CBV (misery perfusion) on the PET images correspond with those of decreased CVR on the SPECT images. The lesions were classified into 3 groups according to their PET-evaluated OEF values, and each value was plotted according to the CBF index at rest and the CVR values obtained in the SPECT study (Figure 5). When the CVR cutoff value was set at 0.23 (mean−2 SD; broken line), the sensitivity of the measurement was 91% (10 of 11), and the specificity was 83% (44 of 53); however, the positive predictive value was only 53% (10 of 19) for detection of lesions with an increased OEF. When the CBF index cutoff value was set at 0.65 (mean−2 SD; dotted line), the sensitivity of the measurement was low (5 of 11, 45%). Therefore, neither the CBF index nor CVR value alone was effective in detecting lesions with an increased OEF. However, when a CVR cutoff value of 0.23 (mean−2 SD) and a CBF index cutoff value of 0.83 (normal value) (thick line) were used, the sensitivity of this combined measurement was 82% (9 of 11), the specificity was 96% (51 of 53), and the positive predictive value was 82% (9 of 11).

Discussion

Because stage 2 cerebral hemodynamic failure, characterized by an elevated OEF and also known as misery perfusion, significantly increases the risks of stroke and ipsilateral ischemic stroke,[2,3] patients with misery perfusion must be detected in clinical practice through the use of widely available modalities such as SPECT. However, a single measurement of CBF alone with SPECT is insufficient to assess the cerebral hemodynamic status in patients with carotid occlusive diseases. Therefore, CVR is usually assessed by paired blood flow measurements, with the initial measurement performed at rest and the second measurement performed after a vasodilatory stimulus such as hypercapnia, an ACZ challenge, or physiological tasks. Although a dissociation between the CBF response to hypercapnia, ACZ, or neural activation has been reported in patients with carotid occlusive disease,[16,17] ACZ increases the arterial-to-capillary blood volume and CBF without changing the $CMRo_2$ and other physiological parameters.[18] Only a few studies have investigated the relationship between ACZ reactivity and OEF.[10,11] Some investigators have reported no significant relationship between O^{15} H_2O PET-measured changes in CBF after an ACZ challenge and quantitative OEF values.[19] Conversely, the most consistent results have been published by Hirano et al,[10] who reported that a reduced regional CVR on IMP SPECT was strongly correlated with an elevated OEF and suggested that a significantly reduced regional CVR represents stage 2 hemodynamic failure with an increased OEF on PET. Hirano et al used conventional ^{123}I-IMP SPECT with arterial sampling and an asymmetry index comparing affected and nonaffected sides after the ACZ test. However, cerebral hemodynamics may be disturbed in the nonaffected hemisphere as a result of collateral circulation, suggesting that the CVR in the contralateral hemisphere cannot be used as an internal control for each patient, even in unilateral

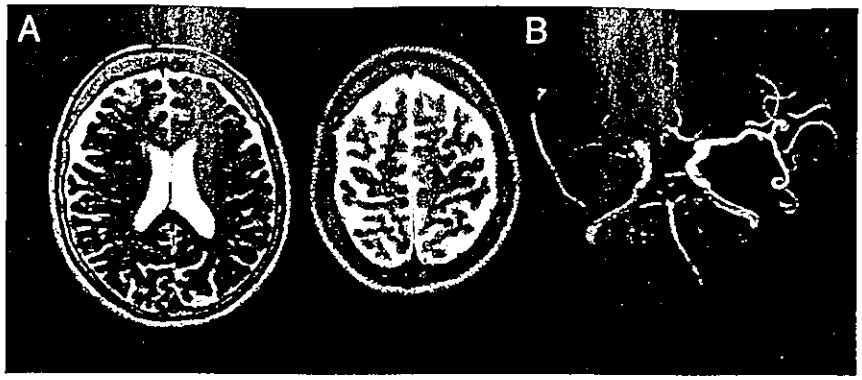

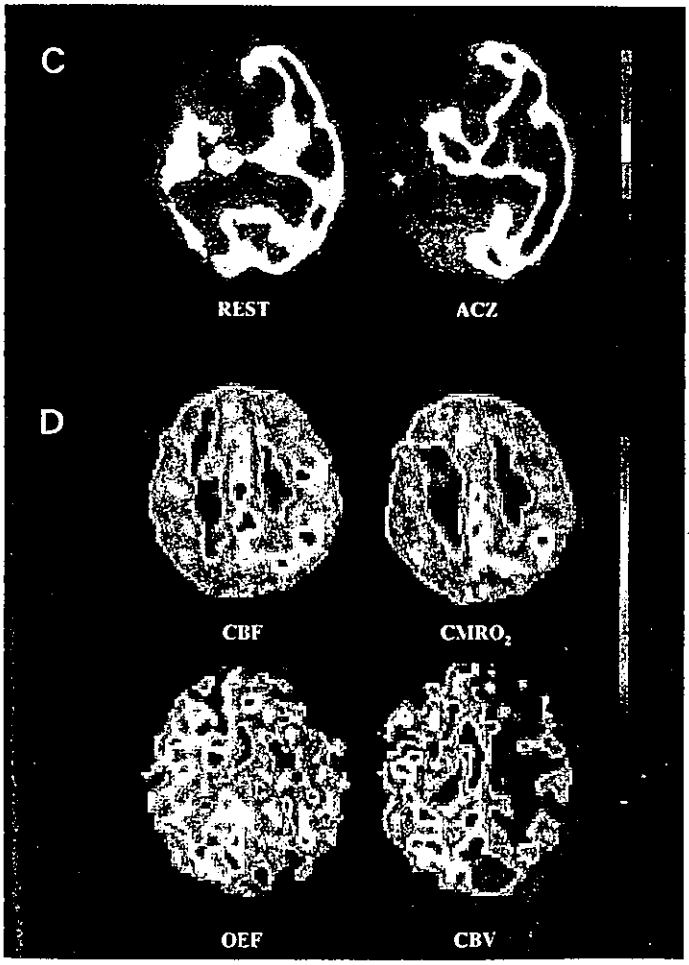

Figure 4. Representative MRI (A), MRA (B), SPECT images (C), and PET images (D) in a patient with misery perfusion (patient 25). This patient is a 69-year-old woman with a right internal carotid occlusion. A, MRI shows no infarction. B, MRA shows occlusion of right internal carotid occlusion. C, SPECT images demonstrate a reduced CBF at rest and a reduced CVR after ACZ challenge in the right cerebral hemisphere (CBF index=0.62, CVR=−0.07). D, PET images demonstrate an elevated OEF and CBV in the right cerebral hemisphere (OEF=61%, CBV=5.8%).

carotid occlusive disease.[20] Furthermore, patients with bilateral carotid disease cannot be evaluated with an asymmetry index for ^{123}I-IMP SPECT after an ACZ challenge.

We have developed a split-dose ^{123}I-IMP SPECT method for evaluating CVR after cerebral vasodilatory stimuli and have modified the procedure so that invasive arterial blood sampling is not required.[6,7,21,22] In contrast to the conventional ^{123}I-IMP SPECT method for measuring CVR, which required arterial sampling and 2 days to perform, our split-dose ^{123}I-IMP SPECT method can be completed in ≈1 hour. During the short interval between the baseline and ACZ challenge tests, the physiological parameters (blood pressure, arterial pH, and $Paco_2$) should be stable, allowing the absolute CVR values to be calculated without arterial blood sampling for quantitative measurement of CBF.

In contrast to Powers'[23] theory, a negative correlation was observed between split-dose ^{123}I-IMP SPECT–measured CVR values and the OEF, suggesting that the OEF may be elevated even at the stage when the CVR response to ACZ is maintained. Several factors may contribute to this correlation between CVR and OEF. First, the OEF may begin to increase before the arteries reach maximal dilatation by autoregulation. This is supported by Derdeyn et al,[24] who observed patients with an increased OEF but without an increased CBV. Second, the vascular systems that dilate after a decrease in cerebral perfusion pressure or in response to an ACZ

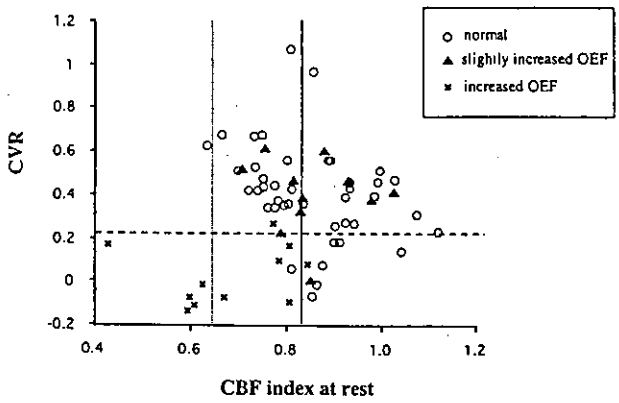

Figure 5. Detection of stage 2 cerebral hemodynamic failure by semiquantitative SPECT analysis on the affected side (group A). The lesions were classified into 3 groups according to their OEF values determined by PET, and each value was plotted on the basis of the CBF index at rest and CVR measured in the SPECT study. Neither the CBF index nor CVR alone was effective in detecting lesions with an elevated OEF. However, when a CVR cutoff value of 0.23 (mean−2 SD; broken line) and a CBF index cutoff value of 0.83 (normal value; thick line) were combined, a sensitivity of 82% (9 of 11), specificity of 96% (51 of 53), and a positive predictive value of 82% (9 of 11) were obtained.

challenge may be different.[17] Third, the ischemic brain tissue within the ROI may be heterogeneous, creating the possibility that regions of stage 1 and 2 hemodynamic failure may be mixed within the same ROI.

On the basis of the correlation between the split-dose ^{123}I-IMP SPECT–measured CVR values and the PET-measured OEF values, we attempted to clarify whether the CVR value alone could predict the existence of misery perfusion. Although the CVR cutoff value showed a high sensitivity (10 of 11, 91%) for the detection of misery perfusion (Figure 5), the positive predictive value was rather low (10 of 19, 53%). Because a significant correlation between CVR and CBF was not found in the PET study (Figure 3), we used the ^{123}I-IMP SPECT–measured CBF index represented as a cerebrum-to-cerebellum ratio to improve the positive predictive value of CVR for detecting misery perfusion. The SPECT-measured CBF index and the PET-measured CBF values were significantly correlated ($n=108$, $r=0.380$, $P<0.001$; data not presented). As expected from the results of Figure 3, the CBF indexes in ROIs below the CVR cutoff value (0.23) varied considerably (from 0.43 to 1.11). However, a combined CVR cutoff value (0.23) and a CBF index cutoff value of 0.83 produced a high sensitivity (9 of 11, 82%), specificity (51 of 53, 96%), and positive predictive value (9 of 11, 82%) for the detection of misery perfusion with an increased OEF (OEF >53.3%), as shown in Figure 5. We determined an abnormal CVR and CBF index with a 95% confidence limit from control subjects in the present study on the basis of the previous studies[3,10,20]; however, the pathophysiological relevance of a CVR and CBF index that is 2 SD from the mean is not necessarily clear and should be clarified in future studies. Five patients with bilateral carotid occlusive diseases were included in this study (the Table), but none of these patients exhibited an elevated OEF on their PET images. However, the combination of the CVR and CBF index (Figure 5) could potentially be applied for the detection of misery perfusion in both unilateral and bilateral carotid occlusive diseases.

In conclusion, split-dose ^{123}I-IMP SPECT can be potentially useful as a cost-effective, noninvasive tool to detect patients with misery perfusion. The combination of the CVR and CBF index can be a reliable index for accurately detecting the existence of increased OEF in both unilateral and bilateral carotid occlusive diseases.

Acknowledgments

We would like to thank the staff of the Department of Nuclear Medicine and the cyclotron staff of Osaka University Medical School Hospital for their technical support in performing the studies.

References

1. Yonas H, Smith HA, Durham SR, Pentheny SL, Johnson DW. Increased stroke risk predicted by compromised cerebral blood flow reactivity. *J Neurosurg.* 1993;79:483–489.
2. Grubb RL Jr, Derdeyn CP, Fritsch SM, Carpenter DA, Yundt KD, Videen TO, Spitznagel EL, Powers WJ. Importance of hemodynamic factors in the prognosis of symptomatic carotid occlusion. *JAMA.* 1998;280: 1055–1060.
3. Yamauchi H, Fukuyama H, Nagahama Y, Nabatame H, Ueno M, Nishizawa S, Konishi J, Shio H. Significance of increased oxygen extraction fraction in five-year prognosis of major cerebral arterial occlusive diseases. *J Nucl Med.* 1999;40:1992–1998.
4. Powers WJ, Press GA, Grubb RL Jr, Gado M, Raichle ME. The effect of hemodynamically significant carotid artery disease on the hemodynamic status of the cerebral circulation. *Ann Intern Med.* 1987;106:27–34.
5. Baron JC, Bousser MG, Rey A, Guillard A, Comar D, Castaigne P. Reversal of focal "misery-perfusion syndrome" by extra-intracranial arterial bypass in hemodynamic cerebral ischemia: a case study with ^{15}O positron emission tomography. *Stroke.* 1981;12:454–459.
6. Hashikawa K, Matsumoto M, Moriwaki H, Oku N, Okazaki Y, Uehara T, Handa N, Kusuoka H, Kamada T, Nishimura T. Split dose iodine-123-IMP SPECT: sequential quantitative regional cerebral blood flow change with pharmacological intervention. *J Nucl Med.* 1994;35: 1226–1233.
7. Hashikawa K, Matsumoto M, Moriwaki H, Oku N, Seike Y, Sakaguchi M, Sugimoto K, Nishimura H, Fukuchi K, Watanabe Y, Uehara T, Hori M, Nishimura T. Non-invasive measurement of cerebral perfusion reserve, split dose I-123 IMP SPECT method: the validation with O-15 H2O PET method. *J Nucl Med.* 1997;38:279. Abstract.
8. Kanno I, Uemura K, Higano S, Murakami M, Iida H, Miura S, Shishido F, Inugami A, Sayama I. Oxygen extraction fraction at maximally vasodilated tissue in the ischemic brain estimated from the regional CO_2 responsiveness measured by positron emission tomography. *J Cereb Blood Flow Metab.* 1998;8:227–235.
9. Herold S, Brown MM, Frackowiak RS, Mansfield AO, Thomas DJ, Marshall J. Assessment of cerebral haemodynamic reserve: correlation between PET parameters and CO_2 reactivity measured by the intravenous 133 xenon injection technique. *J Neurol Neurosurg Psychiatry.* 1988;51: 1045–1050.
10. Hirano T, Minematsu K, Hasegawa Y, Tanaka Y, Hayashida K, Yamaguchi T. Acetazolamide reactivity on ^{123}I-IMP single photon emission computed tomography in patients with major cerebral artery occlusive disease: correlation with positron emission tomography parameters. *J Cereb Blood Flow Metab.* 1994;14:763–770.
11. Nariai T, Suzuki R, Hirakawa K, Maehara T, Ishii K, Senda M. Vascular reserve in chronic cerebral ischemia measured by the acetazolamide challenge test: comparison with positron emission tomography. *AJNR Am J Neuroradiol.* 1995;16:563–570.
12. North America Symptomatic Carotid Endarterectomy Trial Steering Committee. North America Symptomatic Carotid Endarterectomy Trial: methods, patient characteristics and progress. *Stroke.* 1991;22:711–720.
13. Whisnant JP, Basford JR, Bernstein EF. Classification of cerebrovascular disease III. *Stroke.* 1990;21:637–676.
14. Hauge A, Nicolaysen G, Thoresen M. Acute effects of acetazolamide on cerebral blood flow in man. *Acta Physiol Scand.* 1983;117:233–239.

15. Sullivan HG, Allison JD, Kingsbury TB 4th, Goode JJ. Analysis of inhalation rCBF data. *Stroke*. 1987;18:495–502.
16. Kazumata K, Tanaka N, Ishikawa T, Kuroda S, Houkin K, Mitsumori K. Dissociation of vasoreactivity to acetazolamide and hypercapnia: comparative study in patients with chronic occlusive major cerebral artery disease. *Stroke*. 1996;27:2052–2058.
17. Inao S, Tadokoro M, Nishino M, Mizutani N, Terada K, Bundo M, Kuchiwaki H, Yoshida J. Neural activation of the brain with hemodynamic insufficiency. *J Cereb Blood Flow Metab*. 1998;18:960–967.
18. Okazawa H, Yamauchi H, Sugimoto K, Toyoda H, Kishibe Y, Takahashi M. Effects of acetazolamide on cerebral blood flow, blood volume, and oxygen metabolism: a positron emission tomography study with healthy volunteers. *J Cereb Blood Flow Metab*. 2001;21:1472–1479.
19. Hayashida K, Hirose Y, Tanaka Y. Stratification of severity by cerebral blood flow, oxygen metabolism and acetazolamide reactivity in patients with cerebrovascular disease. In: Ishii Y, ed. *Recent Advances in Biomedical Imaging*. Amsterdam, Netherlands: Elsevier; 1997:113–119.
20. Yamauchi H, Fukuyama H, Kimura J, Konishi J, Kameyama M. Hemodynamics in internal carotid artery occlusion examined by positron emission tomography. *Stroke*. 1990;21:1400–1406.
21. Moriwaki H, Matsumoto M, Hashikawa K, Oku N, Ishida M, Seike Y, Watanabe Y, Hougaku H, Handa N, Nishimura T. Hemodynamic aspect of cerebral watershed infarction: assessment of perfusion reserve using iodine-123-iodoamphetamine SPECT. *J Nucl Med*. 1997;38:1556–1562.
22. Moriwaki H, Matsumoto M, Hashikawa K, Oku N, Ishida M, Seike Y, Fukuchi K, Hori M, Nishimura T. Iodine-123-iomazenil and iodine-123-iodoamphetamine SPECT in major cerebral artery occlusive disease. *J Nucl Med*. 1998;39:1348–1353.
23. Powers WJ. Cerebral hemodynamics in ischemic cerebrovascular disease. *Ann Neurol*. 1991;29:231–240.
24. Derdeyn CP, Grubb RL Jr, Powers WJ. Cerebral hemodynamic impairment: methods of measurement and association with stroke risk. *Neurology*. 1999;53:251–259.

AJNR Am J Neuroradiol 23:1356–1358, September 2002

Case Report

Prominent Matched Hypoperfusion in an Intact Cerebellum after a Solitary Middle Cerebellar Peduncle Infarct

Masashi Takasawa, Kazuo Kitagawa, Toshiho Ohtsuki, Naohiko Oku, Kazuo Hashikawa, Saburo Sakoda, Masatsugu Hori, and Masayasu Matsumoto

Summary: We examined the cerebellar metabolism of a 61-year-old man with a small infarct in the left middle cerebellar peduncle and an intact cerebellum. Positron emission tomographic images obtained 28 days after onset showed prominent hypoperfusion and hypometabolism (almost 50% below the normal level) in the left cerebellar hemisphere. This case report shows that neural deafferentation may cause prominent hypometabolism without morphologic changes in the cerebellum. An arrest in synaptic activity may be the most important factor for the adaptive decrease in oxygen metabolism seen in ischemic brain.

Cerebral blood flow and oxygen metabolism can be measured by using positron emission tomography (PET), thanks to the high spatial resolution and accurate quantitation characteristics of this technique. Intensive examination of patients with acute stroke has shown that the threshold of oxygen metabolism required for tissue survival in an ischemic condition is approximately 50% of the normal level (1–4). In other words, the brain has an intrinsic adaptive mechanism against ischemic insults that involves a reduction in oxygen metabolism. Cerebral vasodilatation and an increased uptake of oxygen are well known to be adaptive responses of the brain to a reduction in perfusion pressure (5, 6). However, the mechanism for the adaptive decrease in oxygen metabolism has not been previously discussed. Because a 50% reduction in oxygen metabolism in the surviving tissue is unexpectedly high and almost identical to the effect of hypothermia at 32°C (7), the elucidation of this adaptive response is important for improving our understanding of the pathophysiology of acute stroke and the development of novel therapeutic strategies. The disconnection of synaptic circuits may be an important component of this mechanism, because electrical activity is arrested, but energy metabolism is preserved in the penumbra tissue (4, 8).

In humans, a reduction in oxygen metabolism without any morphologic change occurring after supratentorial infarction is known as *crossed cerebellar diaschisis* (9). This form of hypometabolism is presumably caused by an interruption in the cerebropontocerebellar pathway. Because the degree of oxygen metabolism reduction varies between 0 and 37% according to the size and location of the supratentorial infarction (10, 11), it remains uncertain to what degree the disconnection of synaptic circuits reduces oxygen metabolism in the intact brain. We had the opportunity to examine cerebellar circulation and metabolism in a case with a solitary middle cerebellar peduncle infarct, in which most afferent and efferent fibers to the cerebellum were disconnected.

Case Report

A 61-year-old, right-handed man suddenly presented with severe gait unsteadiness and vomiting. Hypertension and impaired glucose tolerance had been diagnosed when the patient was 50 years old, but the patient did not undergo treatment. The diagnosis of cerebellar infarction was made on the basis of neurologic findings at another hospital. He was transferred to our hospital 3 weeks after onset. A neurologic examination performed at admission showed left-sided ataxia and ataxic speech. Both the nose-finger-nose test and the pronation-supination test performances were clumsy on the left side. No signs of ipsilateral facial palsy, hearing loss, trigeminal sensory loss, or Horner syndrome were observed. After admission, the neurologic findings did not deteriorate, and the patient showed gradual improvement. Informed consent to participate in this study was obtained from the patient and his family.

An MR imaging examination was performed on the 24th day after onset and revealed an infarct in the left middle cerebellar peduncle (Fig 1, *arrow*), located within the territory of the anterior inferior cerebellar artery. MR diffusion- and perfusion-weighted images were not obtained. No definite infarcts were found in the cerebral hemisphere or the left cerebellar hemisphere on T1- or T2-weighted images. Cerebral angiography was not performed. MR angiography showed no definite stenosis and only slight atherosclerotic changes in the bilateral vertebral arteries and the basilar artery.

PET was performed by using a Headtome V scanner (Shimadzu Corp., Kyoto, Japan) on the 28th day after symptom onset. The PET examination was performed according to steady-state methods by using ^{15}O-labeled gases. Regional cerebral blood flow, cerebral metabolic oxygen rate, cerebral blood volume, and oxygen extraction fraction were measured.

Received February 20, 2002; accepted after revision March 18.

From the Department of Neurology and Cerebrovascular Disease (M.T., K.K., T.O., N.O., K.H., S.S., M.M.), Osaka University Hospital, the Division of Strokology (M.T., K.K., T.O., M.H., M.M.), Department of Internal Medicine and Therapeutics, Osaka University Graduate School of Medicine, and the Department of Nuclear Medicine (N.O., K.H.), Osaka University Graduate School of Medicine, Osaka, Japan.

Address reprint requests to Masashi Takasawa, MD, Division of Strokology, Department of Internal Medicine and Therapeutics, Osaka University Graduate School of Medicine, 2-2, Yamadaoka, Suita City, Osaka, 565-0871, Japan.

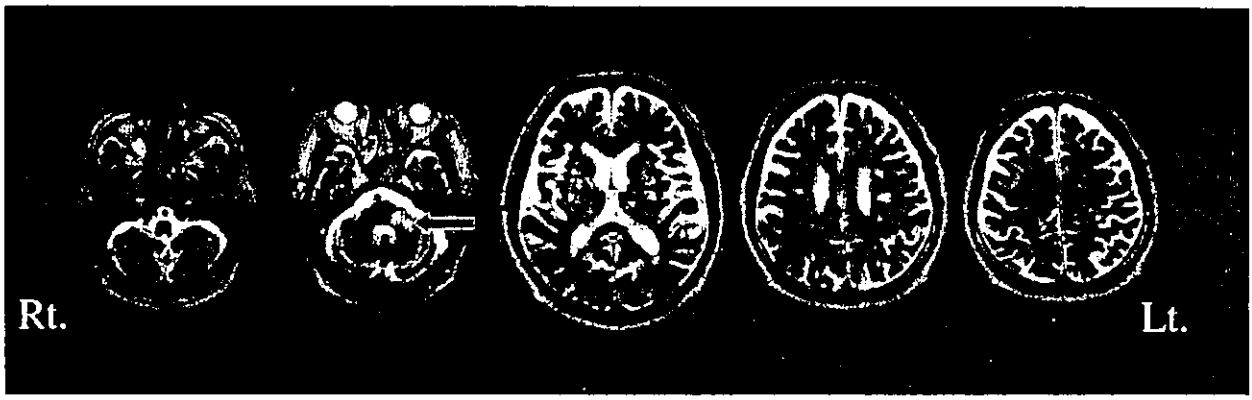

FIG 1. MR images obtained 24 days after symptom onset show an infarct strictly confined to the left middle cerebellar peduncle (*arrow*). No definite infarctions are visible in the cerebral hemisphere or the left cerebellar hemisphere on T2-weighted images. *Rt.*, right; *Lt.*, left.

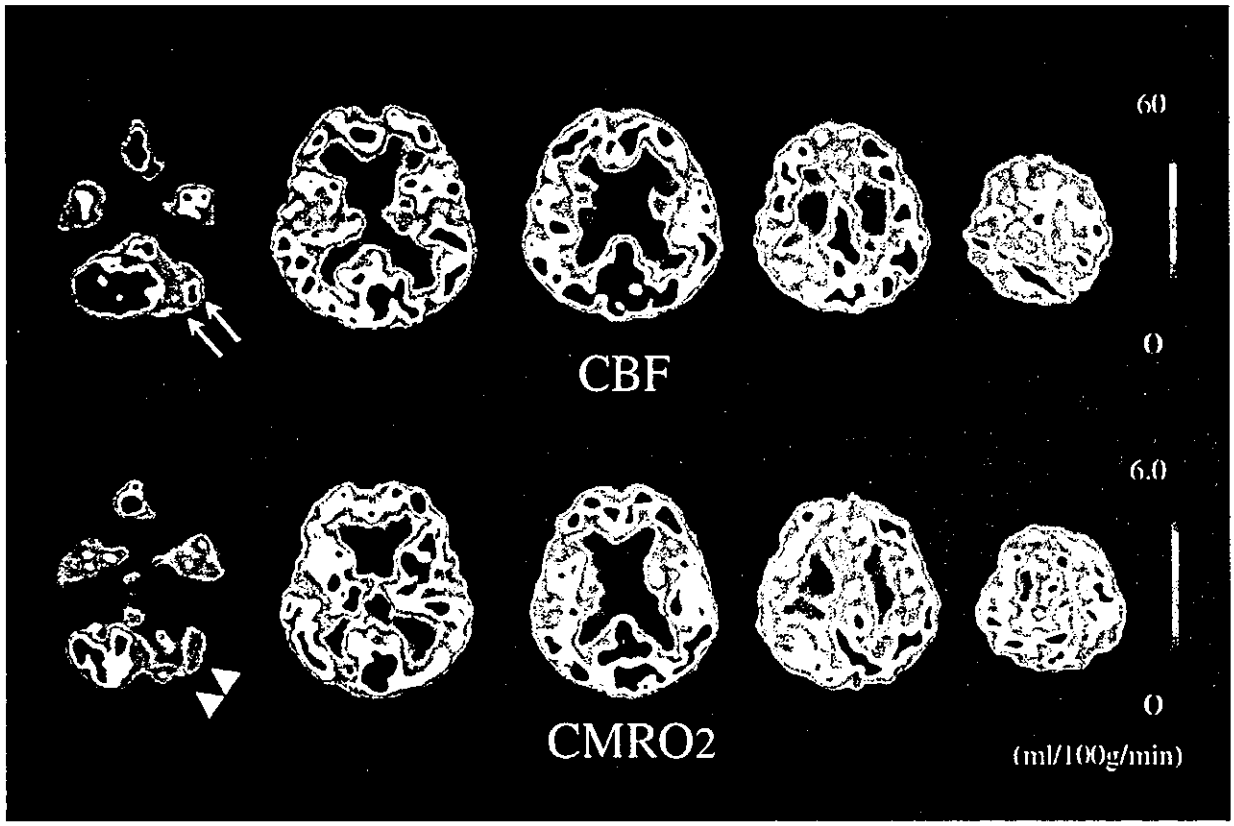

FIG 2. Positron emission tomographic images obtained 28 days after symptom onset show severe hypoperfusion (*arrows*) and oxygen hypometabolism (*arrowheads*) in the left cerebellar hemisphere. *CBF*, cerebral blood flow; $CMRO_2$, cerebral metabolic oxygen rate.

Circular regions of interest, 20 mm in diameter, were placed on the cerebellar hemispheres in the PET images.

The PET images showed severe hypoperfusion (right, 68.9 mL/100 mg/min; left, 35.7 mL/100 mg/min) (Fig 2, *arrows*) and hypometabolism (right, 4.45 mL/100 mg/min; left, 2.75 mL/100 mg/min) (Fig 2, *arrowheads*) in the left cerebellar hemisphere. Elevated oxygen extraction fraction values, which have been shown in cases of misery perfusion (5), were not observed in bilateral cerebellar hemispheres (right, 38.6%; left, 40.5%). The standard PET parameters in the cerebelli of normal controls examined at our hospital's PET center are 63 ± 6.5 mL/100 mg/min for cerebral blood flow (mean ± SD), 4.3 ± 0.6 mL/100 mg/min for cerebral metabolic oxygen rate, and 46 ± 4.0% for oxygen extraction fraction in a cerebellar hemisphere.

Discussion

Quantitative cerebral blood flow mapping by using PET has revealed the remote effects of focal cerebral lesions in humans. The phenomenon of cerebellar hypoperfusion and hypometabolism occurring after supratentorial infarction, termed *crossed cerebellar diaschisis*, occurs via the cerebropontocerebellar pathway and was first described by Baron et al (9).

The cerebellum is linked to other parts of the brain by numerous efferent and afferent fibers that are grouped together on each side of the cerebellum into

three peduncles. The middle cerebellar peduncle is the largest of the three peduncles and arises from the posterolateral region of the pons; it consists of the transverse fibers of the pons, which arise from the neurons of the pontine nuclei (12). In our patient, the interception of most efferent and afferent fibers of the cerebellar hemisphere by a middle cerebellar peduncle infarct resulted in profound hypoperfusion (almost 50% lower than the nonaffected cerebellar hemisphere) and profound hypometabolism (almost 40% lower), without any signs of morphologic change. The severity of this hypoperfusion and hypometabolism was greater than that reported previously regarding human study participants and was almost the same as the ischemic reversible threshold (4, 6, 13).

In cases of acute stroke, PET studies have been used to document the existence of a penumbra (4, 14) in which the electrocorticogram and evoked potentials vanish but the membrane potential and energy metabolism are maintained (4, 8). In this penumbra, ischemic tissue can survive for several hours under conditions of reduced oxygen consumption (almost 50% of normal) and recovers if adequate recirculation occurs (4). Surprisingly, the maximum level of oxygen consumption suppression in the penumbra is nearly identical to that in the cerebellum in the presence of a solitary middle cerebellar peduncle infarct.

Disconnection of the efferent and afferent fibers to the cerebellum suppressed the level of oxygen metabolism by approximately 40% in the present study. These findings seem to agree with previous findings of autoradiography that entorhinotomy in experimental animals causes a 30% to 45% reduction in glucose metabolism in the hippocampus (15). Because the cerebral metabolic oxygen rate threshold for irreversible injury in the ischemic brain has been found to be approximately 40% to 50% of normal (16), the adaptive decrease in oxygen consumption in the penumbra may be ascribed to the disconnection of synaptic circuits, although other mechanisms, such as the inhibition of protein synthesis, could also preserve oxygen consumption (17).

Conclusion

The mechanism by which EEG and electrical activity is suppressed remains uncertain, but suppression of the conduction action potential in the axons of afferent fibers under ischemic conditions (18) may be important for functional depression. The present study suggests that disconnection of the synaptic circuit into the ischemic brain may further reduce the cerebral metabolic oxygen rate threshold for irreversible injury.

Acknowledgments

The authors thank the staff of the Department of Nuclear Medicine and the Cyclotron staff of Osaka University Medical School Hospital for technical support in performing the studies and R. Morimoto and S. Imoto for administrative assistance.

References

1. Baron JC, Rougemont D, Bousser MG, Lebrun-Grandie P, Iba-Zizen MT, Chiras J. **Local CBF, oxygen extraction fraction (OEF), and $CMRO_2$: prognostic value in recent supratentorial infarction in humans.** *J Cereb Blood Flow Metab* 1983;3[suppl 1]:S1–S2
2. Powers WJ, Grubb RL Jr, Darriet D, Raichle ME. **Cerebral blood flow and cerebral metabolic rate of oxygen requirements for cerebral function and viability in humans.** *J Cereb Blood Flow and Metab* 1985;5:600–608
3. Ackerman RH, Lev MH, Mackay BC, et al. **PET studies in acute stroke: findings and relevance to therapy.** *J Cereb Blood Flow Metab* 1989;9[suppl 1]:S359
4. Heiss WD. **Ischemic penumbra: evidence from functional imaging in man.** *J Cereb Blood Flow Metab* 2000;20:1276–1293
5. Baron JC, Bousser MG, Rey A, Guillard A, Comar D, Castaigne P. **Reversal of focal "misery-perfusion syndrome" by extra-intracranial arterial bypass in hemodynamic cerebral ischemia.** *Stroke* 1981;12:454–459
6. Powers WJ, Press AW, Grubb RL Jr, Gado M, Raichle ME. **The effect of hemodynamically significant carotid artery disease on the hemodynamic status of the cerebral circulation.** *Ann Intern Med* 1987;106:27–35
7. Metz C, Holzschuh M, Bein T, et al. **Moderate hypothermia in patients with severe head injury: cerebral and extracerebral effects.** *J Neurosurg* 1996;85:533–541
8. Baron JC. **Perfusion thresholds in human cerebral ischemia: historical perspective and therapeutic implications.** *Cerebrovasc Dis* 2001;11[suppl 1]:2–8
9. Baron JC, Bousser MG, Comar D, Castaigne P. **"Crossed cerebellar diaschisis" in human supratentorial brain infarction.** *Trans Am Neurol Assoc* 1980;105:459–461
10. Martin WR, Raichle ME. **Cerebellar blood flow and metabolism in cerebral hemisphere infarction.** *Ann Neurol* 1983;14:168–176
11. Pantano P, Baron JC, Samson Y, Bousser MG, Derouesne C, Comar D. **Crossed cerebellar diaschisis: further studies.** *Brain* 1986;109:677–694
12. Carpenter MB, Sutin J. **The cerebellum.** In: Carpenter MB, Sutin J, eds. *Human Neuroanatomy.* 8th ed. Baltimore: Lippincott William & Wilkins; 1983:474–492
13. Heiss WD, Kracht L, Grond M, et al. **Early [^{11}C] flumazenil/H2O positron emission tomography predicts irreversible ischemic cortical damage in stroke patients receiving acute thrombolytic therapy.** *Stroke* 2000;31:366–369
14. Astrup J, Siesjo BK, Symon L. **Thresholds in cerebral ischemia - the ischemic penumbra.** *Stroke* 1981;12:723–725
15. Jorgenesen MB, Wright DC. **The effect of unilateral and bilateral removal of the entorhinal cortex on the glucose utilization in various hippocampal regions in the rat.** *Neurosci Lett* 1988;87:227–232
16. Enblad P, Frykholm P, Valtysson J, et al. **Middle cerebral artery occlusion and reperfusion in promates monitored by microdialysis and sequential positron emission tomography.** *Stroke* 2001;32:1574–1580
17. Hossmann KA. **Viability thresholds and the penumbra of focal ischemia.** *Ann Neurol* 1994;36:557–565
18. Stys PK. **Anoxic and ischemic injury of myelinated axons in CNS white matter: from mechanistic concepts to therapeutics.** *J Cereb Blood Flow Metab* 1998;18:2–25

Journal of Neuroscience Research 69:750–756 (2002)

Differential Expression of Musashi1 and Nestin in the Adult Rat Hippocampus After Ischemia

Yoshiki Yagita,[1] Kazuo Kitagawa,[1]* Tsutomu Sasaki,[1] Takaki Miyata,[2] Hideyuki Okano,[2] Masatsugu Hori,[1] and Masayasu Matsumoto[3]

[1]Division of Strokology, Department of Internal Medicine and Therapeutics, Osaka University Graduate School of Medicine, Osaka, Japan

[2]Department of Physiology, Keio University School of Medicine, Tokyo, Japan

[3]Department of Clinical Neuroscience and Therapeutics, Hiroshima University Graduate School of Biomedical Sciences, Hiroshimna, Japan

Both nestin and the neural RNA-binding protein Musashi1 (Msi1) are expressed in neural stem cells in the subventricular zone. Neurogenesis in the hippocampus has received much attention, so we evaluated the expression of Msi1 and nestin in the adult rat hippocampus after transient forebrain ischemia. Both Msi1 and nestin were induced in the reactive astrocytes after ischemia, especially in the CA1 region, until 35 days after ischemia. Induction of both molecules suggested that reactive astrocytes might have immature characteristics. In the subgranular zone (SGZ) of the hippocampal dentate gyrus, Msi1-positive cells formed clusters after ischemia. These cells were labeled by bromodeoxyuridine (BrdU) but did not express glial fibrillary acidic protein. In contrast, very few nestin-positive cells were labeled by BrdU. Our results suggest that neuronal progenitor cells in the SGZ expressed Msi1 but not nestin.

Key words: hippocampus; ischemia; neurogenesis; nestin; Musashi-1 (Msi1)

Neural stem/progenitor cells remain in the adult mammalian brain (Reynolds and Weiss, 1992; Weiss et al., 1996; Johansson et al., 1999; Doetsch et al., 1999), including human brain (Pincus et al., 1998). Neurogenesis continues throughout life in the two restricted zones, the hippocampal subgranular zone (SGZ; Altman and Das, 1965, 1967; Gould et al., 1998; Eriksson et al., 1998) and the rostral migratory stream, where newly generated immature neurons migrate from the anterior subventricular zone (SVZ) into the olfactory bulb (Lois and Alvarez-Buylla, 1994). It has been reported that brain injury stimulates neurogenesis in the SGZ and SVZ. Mechanical injury to the dentate gyrus (Gould and Tanapat, 1997), olfactory bulbectomy (Kirschenbaum et al., 1999), seizure (Parent et al., 1997), and ischemia (Liu et al., 1998; Takagi et al., 1999; Kee et al., 2001; Jin et al., 2001; Yoshimura et al., 2001) can affect cell proliferation in these neurogenic regions. Although in situ detection of neuronal progenitor cells is necessary to understand their response in vivo, no specific markers are available with which to detect progenitor cells.

Both Musashi1 (Msi1) and nestin are considered selective markers for neural stem/progenitor cells. Msi1 was primarily isolated as the required molecule for asymmetric division of sensory organ precursor cells in *Drosophila* (Nakamura et al., 1994). Msi1 posttranscriptionally regulates *numb* gene expression, which is involved in Notch signaling (Imai et al., 2001). In the adult mammalian brain, Msi1 is present in the ependymal cells, subependymal cells, and astrocytes but not in the microglia, oligodendrocyte, or mature neurons (Sakakibara et al., 1996; Sakakibara and Okano, 1997; Kaneko et al., 2000). We recently demonstrated that the cluster-forming proliferative cells in the SGZ after transient forebrain ischemia and after permanent focal ischemia express Msi1 but not glial fibrillary acidic protein (GFAP; Yagita et al., 2001; Takasawa et al., 2002).

Nestin was originally identified as an antigen of monoclonal antibody RAT401, which was raised against embryonic spinal cord (Hockfield and McKay, 1985; Lendahl et al., 1990). It is an intermediate filament expressed in the germinal zone and has been widely used as a neuronal stem/progenitor cell marker. The expression profile of nestin after brain injury, including ischemia, has been studied intensively. Interestingly, after injury, reactive astrocytes express nestin immunoreactivity (Clarke et al., 1994; Lin et al., 1995; Duggal et al., 1997; Li and Chopp, 1999). Given that SVZ and SGZ astrocytes have been identified as precursor cells (Doetsch et al., 1999; Seri et al., 2001), these findings may suggest that reactive

*Correspondence to: Dr. Kazuo Kitagawa, Division of Strokology, Departement of Internal Medicine and Therapeutics (A8), Osaka University Graduate School of Medicine, 2-2 Yamadaoka, Suita City, Osaka 565-0871, Japan. E-mail: kitagawa@medone.med.osaka-u.ac.jp

Received 20 February 2002; Revised 10 March 2002; Accepted 3 April 2002

Published online in Wiley InterScience (www.interscience.wiley.com). DOI: 10.1002/jnr.10342

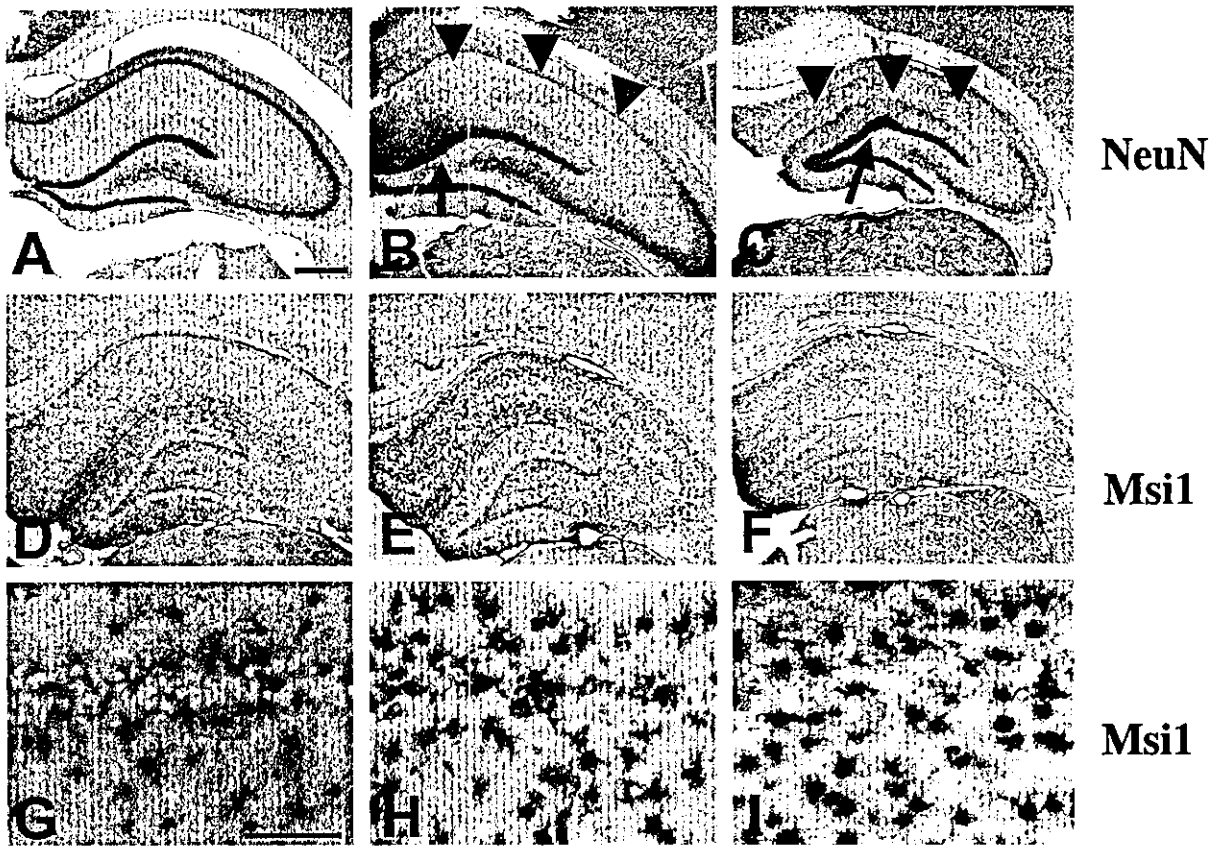

Fig. 1. Neuronal death and Msi1 expression in the hippocampus after transient forebrain ischemia. **A–C:** NeuN immunohistochemistry. In the nonischemic hippocampus, NeuN was expressed in the pyramidal layer, dentate gyrus, and interneurons (A). Seven (B) and thirty-five (C) days after ischemia, NeuN immunoreactivity disappeared in the CA1 (arrowheads) and CA4 (arrows) regions. **D–I:** Msi1 immunohistochemistry in the whole hippocampus (D–F) or CA1 region (G–I). In the control brain, Msi1-positive cells were observed throughout the whole hippocampus (D,G). The Msi1 signal increased 7 days after ischemia (E,H). Signal intensity in the CA1 region was stronger than that in the other hippocampal regions. Msi1 signal in the CA1 region was still stronger than that in the other regions 35 days after ischemia (F,I). Scale bars = 0.5 mm in A (for A–F); 50 μm in G (for G–I).

astrocytes in the mature brain have the potential ability to revert to an undifferentiated stage. However, the expression of nestin in the SGZ has not been studied.

In the present study, we investigated Msi1 expression in the hippocampus after transient forebrain ischemia and compared it with that of nestin and other cell markers. We demonstrated that progenitor cells in the SVZ were labeled with both Msi1 and nestin but that those in the SGZ were labeled only with Msi1.

MATERIALS AND METHODS

Animal Model

Adult male Wistar rats (3–4 months or 1 year old) were used in this study. The experimental protocol was approved by the Institutional Animal Care and Use Committee of Osaka University Graduate School of Medicine. Transient forebrain ischemia was induced by four-vessel occlusion and reperfusion as previously described (Yagita et al., 2001). Both vertebral arteries of rats were cauterized using an electrocautery needle with pentobarbital (45 mg/kg i.p.) anesthesia. On the following day, rats were anesthetized with 1% halothane inhalation, and both common carotid arteries were occluded with miniature aneurysmal clips for 10 min. Rectal temperature was maintained at 37°C and 37.5°C with an overhead heating lamp for up to 1 hr after removal of the clips. We also monitored the skull temperature with a needle thermometer probe placed on the parietal area of the skull and maintained it at 36.0°C during ischemia. Sham-operated animals only went through the first-day procedure and carotid exposure without clipping.

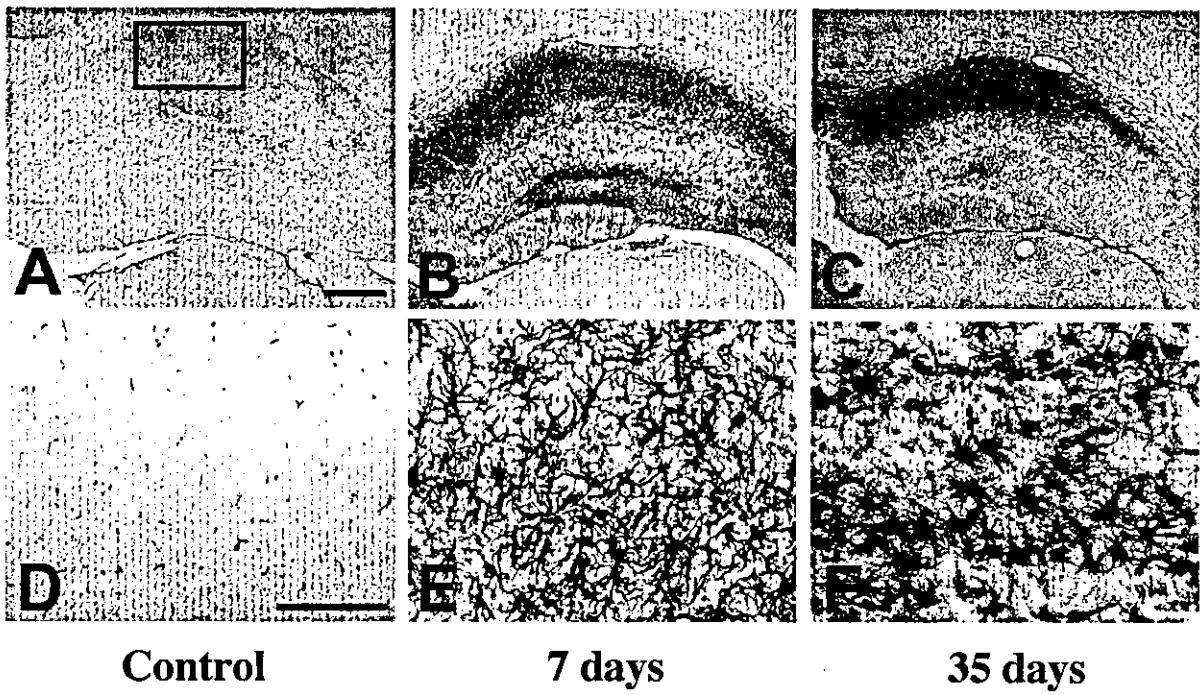

Fig. 2. Nestin expression in the hippocampus after transient forebrain ischemia. **A–C:** Nestin immunohistochemistry in the whole hippocampus. **D–F:** Higher magnification of CA1 regions (boxed area in A). The vascular shape was lightly labeled, but there were few nestin-positive cells in the nonischemic hippocampus (A,D). Seven days after ischemia, many nestin-positive cells appeared throughout the whole hippocampus (B,E). Nestin-positive cells with a round shape were still observed in the CA1 region 35 days after ischemia (C,F). Scale bars = 0.5 mm for in A (A–C); 50 μm in D (for D–F).

Immunohistochemistry

Rats were killed 7 or 35 days after ischemia or sham operation and were perfused with 4% paraformaldehyde. At least 4 rats were used for each time point. The brains were dissected out and cut into coronal blocks containing the hippocampus and immediately immersion fixed in the same fixative at 4°C overnight. Coronal sections (30 μm thick) were cut on a vibratome.

The free-floating brain sections were incubated with a primary antibody at 4°C overnight. Secondary antibody reaction was carried out for 1 hr at room temperature. We used the streptavidin-biotin-peroxidase complex system (Vector, Burlingame, CA) or the peroxidase-linked antiperoxidase system (Cappel, West Chester, PA) to detect primary antibodies and visualized them by reaction with diaminobenzidine and hydrogen peroxide. We used the following antibodies as primary antibodies: rat monoclonal anti-Msi1 antibody (Kaneko et al., 2000), mouse monoclonal anti-NeuN antibody (Chemicon, Temecula, CA; 1:200), mouse monoclonal antinestin antibody (RAT401; Chemicon, 1:200), and rabbit polyclonal anti-GFAP antibody (Sigma, St. Louis, MO; 1:200).

Double immunostaining was analyzed using immunofluoresence and Zeiss confocal microscopy. After the primary antibody reaction described above, sections were incubated with fluorescein isothiocyanate (FITC)-labeled goat anti-mouse or rat IgG antibodies and rhodamine-labeled goat anti-rabbit or rat IgG antibodies.

Bromodeoxyuridine Labeling

We used bromodeoxyuridine (BrdU; Boehringer Mannheim, Mannheim, Germany) to label proliferating cells. Rats received BrdU (50 mg/kg i.p.) three times every 4 hr over a period of 8 hr on the day before sacrifice. On the next day, rats were perfused transcardially with 4% paraformaldehyde and were immersed in the same fixative at 4°C overnight. Free-floating sections were treated in 50% formamide and a 2× saline-sodium citrate buffer at 65°C for 2 hr. After washing in the 2× saline-sodium citrate buffer, sections were incubated in 2 N HCl at 37°C for 30 min. Sections were incubated with mouse monoclonal anti-BrdU antibody (Amersham, Piscateway, NJ; 1:100) and rat monoclonal anti-Msi1 antibody at 4°C overnight.

RESULTS

Almost all pyramidal neurons in the CA1 and a part of the interneurons in the hilus had degenerated following transient forebrain ischemia (Fig. 1A–C). In the hippocampus of normal and sham-operated rats, Msi1 expression was observed throughout the hippocampus (Fig. 1D). Msi1 was located in the nuclei and cytoplasm around the nuclei of glial cells (Fig. 1G). Msi1 expression was up-regulated in the CA1 region 7 days after ischemia (Fig. 1E,H), and increased Msi1 expression was still observed 35 days after ischemia (Fig. 1F,I). Unlike the case with Msi1,

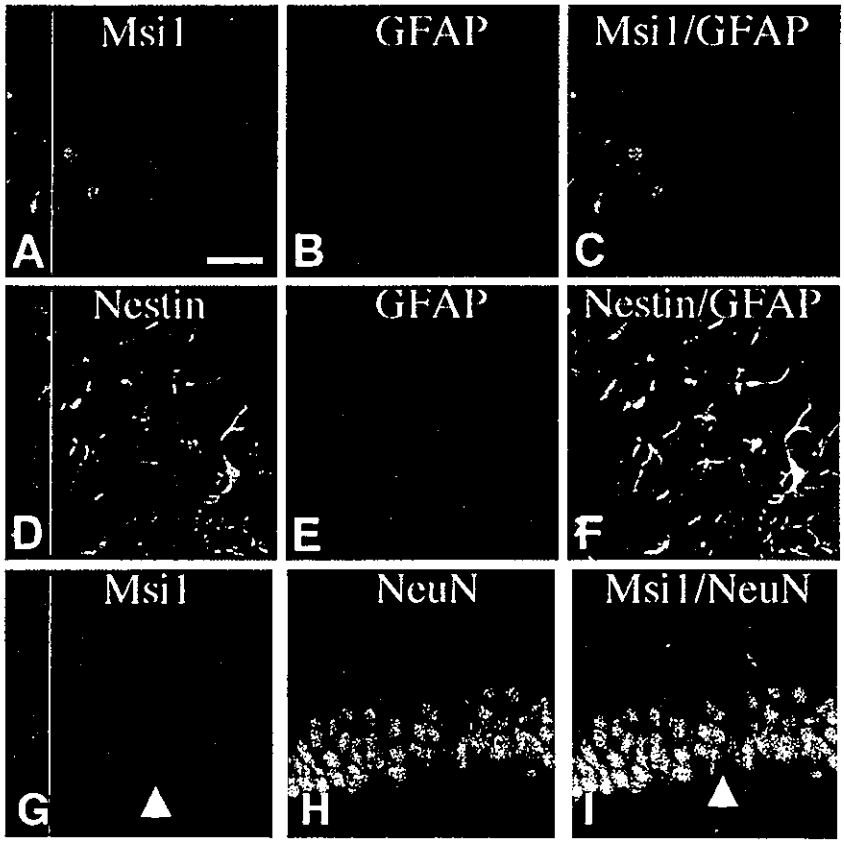

Fig. 3. Msi1 and nestin colocalized with GFAP in the CA1 region after ischemia. To confirm the cell type of Msi1- or nestin-expressing cells, we carried out double immunolabeling. GFAP-positive reactive astrocytes in the CA1 expressed both Msi1 (A–C) and nestin (D–F) 7 days after ischemia. In contrast, Msi1-positive cells did not express NeuN in the normal CA1 region (arrowheads in G,I). **A:** Msi1 (green). **B,E:** GFAP (red). **C:** Msi1/GFAP. **D:** Nestin (green). **F:** nestin/GFAP. **G:** Msi1 (red). **H:** NeuN (green). **I:** Msi1/NeuN. Scale bar = 30 μm

there was only slight nestin immunoreactivity, except for a vascular shape in the nonischemic hippocampus (Fig. 2A,D). Nestin immunoreactivity was markedly increased 7 days after ischemia, especially in the CA1 and CA4 regions (Fig. 2B,E), and up-regulation of nestin immunoreactivity continued in the restricted CA1 region even 35 days after ischemia (Fig. 2C,F). Almost all Msi1 and nestin immunoreactvity was colocalized with GFAP in the CA1 region after ischemia (Fig. 3); reactive astrocytes expressed these two marker proteins of neuronal stem/progenitor cells. In contrast, Msi1 immunoreactvity was not observed in mature NeuN-positive neurons (Fig. 3).

Both Msi1 and nestin were expressed in the ependymal cells and SVZ (Fig. 4). BrdU-positive proliferating cells were found mainly in the SVZ, and they were labeled with both Msi1 and nestin (Fig. 4). However, the BrdU-positive cells in the SGZ were labeled with only Msi1 (Fig. 5A–C) and not with nestin (Fig. 5D–F) in the normal rats and in the rats 7 days and 35 days after ischemia. In the SGZ, Msi1-positive cells did not colocalize with GFAP, whereas almost all nestin-positive cells expressed GFAP in the SGZ (Fig. 6). In contrast, Msi1-positive cells in the hilus colocalized with GFAP (Fig. 6A–C, thin arrows).

DISCUSSION

In the present study, we demonstrated the expression profile of Msi1 and nestin in the hippocampus after transient forebrain ischemia. Both proteins were induced in astrocyte in the CA1 region, where neuronal death has occurred, and up-regulation was sustained for at least 35 days after ischemia. Our present finding is compatible with the hypothesis that reactive astrocyte could revert to an immature state. Recently, Seri et al. (2001) reported that astrocytes in the SGZ generate neuronal precursor cells, which differentiated to granule neuron. Although it is still unclear whether every astrocyte, even in nonneurogenic regions, can function as a neuronal progenitor cell, astrocyte may be a target for novel therapy to replace injured neurons.

It has been reported that nestin is induced in the reactive astrocyte by ischemia (Lin et al., 1995; Duggal et al., 1997; Li and Chopp, 1999), mechanical injury (Kaya et al., 1999), and glutamate toxicity (Clarke et al., 1994). After focal ischemia, nestin was strongly induced around the infarct region in the acute phase (Duggal et al., 1997), and it was sustained for 28 days after ischemia (Li and Chopp, 1999). After transient global ischemia, nestin was expressed in the reactive astrocytes in the hippocampus (Lin et al., 1995). In addition to Msi1 and nestin, RC2 has been shown in neuronal stem/progenitor cells, and it is also expressed in the reactive astrocytes (Sakakibara and Okano, 1997; Leavitt et al., 1999). On the other hand, reactive astrocytes can express highly polysialylated neural

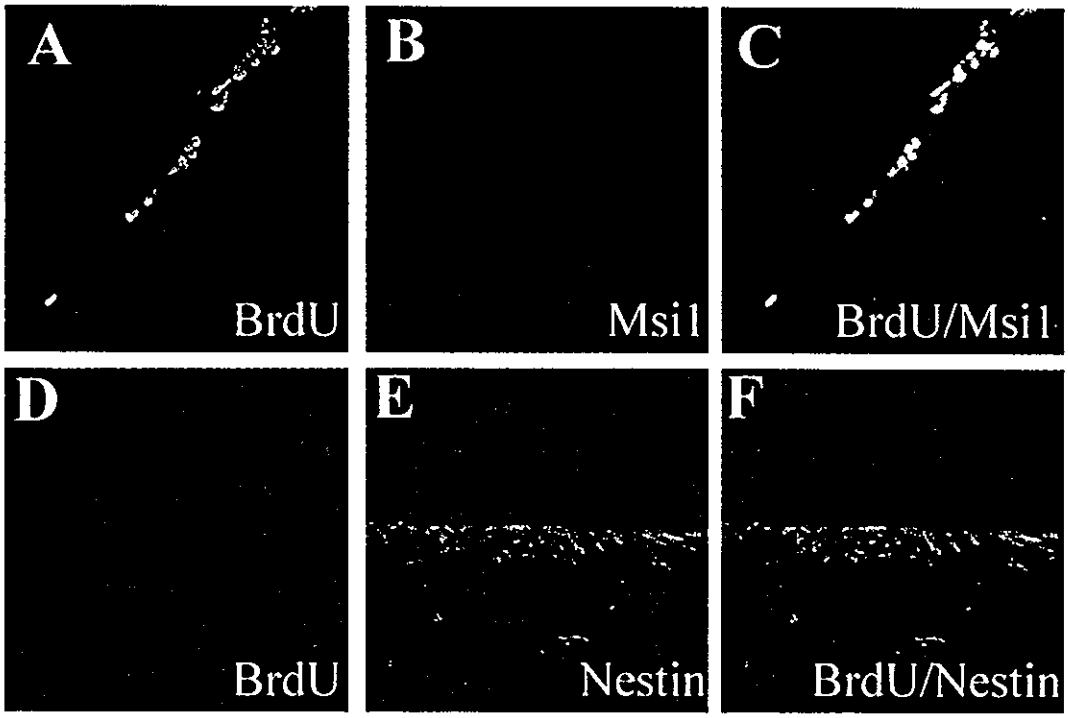

Fig. 4. Proliferating neuronal progenitor cells in the SVZ after ischemia expressed both Msi1 and nestin. BrdU-positive cells were observed in the SVZ (A,D). Both Msi1 (B) and nestin (E) immunoreactivity were observed in the ependymal line and SVZ. BrdU-positive cells in the SVZ expressed both Msi1 and nestin (C,F). **A:** BrdU (green). **B:** Msi1 (red). **C:** BrdU/Msi1. **D:** BrdU (red). **E:** Nestin (green). **F:** BrdU/nestin.

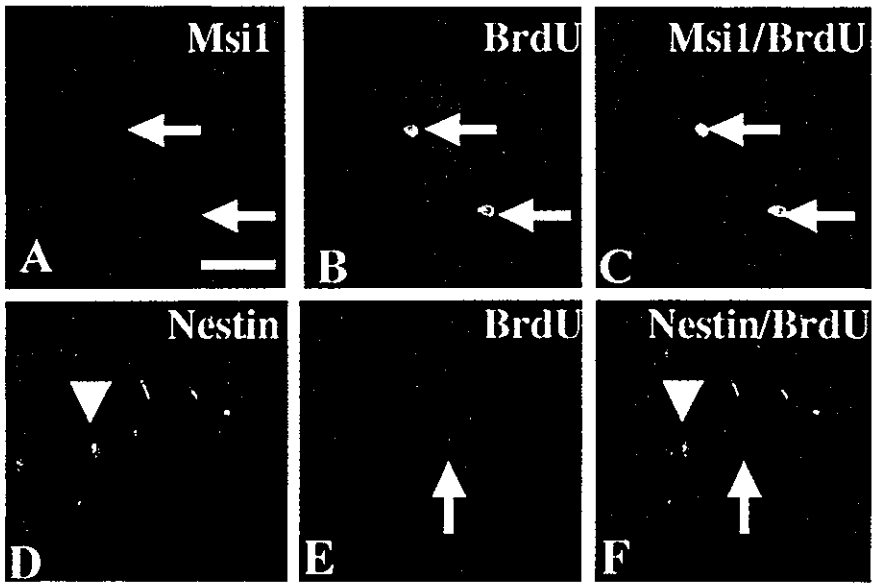

Fig. 5. Visualization of proliferating neuronal progenitor cells in the SGZ with anti-Msi1 antibody. Proliferating cells in the SGZ after ischemia were labeled by BrdU. Cluster-forming BrdU-positive cells expressed Msi1 (arrows in A–C); however, BrdU-positive cells did not express nestin (arrows and arrowheads in D–F). **A:** Msi1 (red). **B:** BrdU (green). **C:** Msi1/BrdU. **D:** Nestin (green). **E:** BrdU (red). **F:** Nestin/BrdU. Scale bar = 30 μm.

cell adhesion molecule (PSA-NCAM) after transient forebrain ischemia (Fox et al., 2001). As with Msi1 and nestin, expression of PSA-NCAM was sustained in the CA1 region in the chronic phase after ischemia. In the normal brain, this molecule was expressed only in immature neurons, which extend neurites (Seki and Arai, 1993), and also in migrating neuroblasts of the SVZ (Lois et al., 1996). After entorhinal cortex lesions, PSA-NCAM was reex-

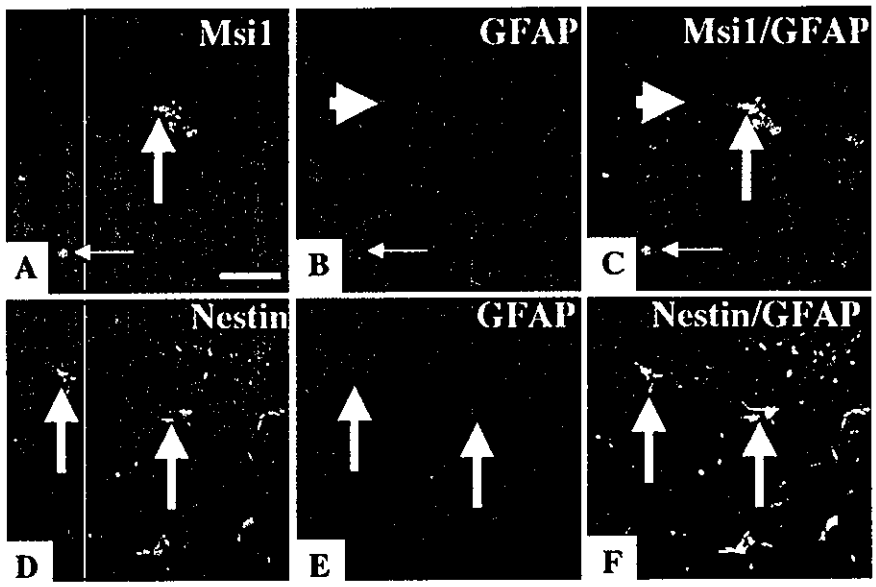

Fig. 6. Cluster-formed Msi1-positive cells did not express GFAP. In the proliferating cells of the SGZ, Msi1 immunoreactivity was not colocalized with GFAP (thick arrows and arrowheads in A–C). However, Msi1-positive cells in the hilus colocalized with GFAP (thin arrows in A–C). All nestin-positive cells expressed GFAP in the SGZ (arrows in D–F) and hilus. **A:** Msi1 (green). **B:** GFAP (red). **C:** Msi1/GFAP. **D:** Nestin (green). **E:** GFAP (red). **F:** Nestin/GFAP. Scale bar = 30 μm.

pressed in denervated dendrites in the outer molecular layer of the dentate gyrus (Styren et al., 1994). Although the role of PSA-NCAM in the reactive astrocyte is still unclear, it may reveal an aspect of an immature state.

Nestin has been widely used as a marker for neuronal stem/progenitor cells (Lendahl et al., 1990); however, very few reports describe nestin immunoreactivity of the neuronal progenitor cells in the SGZ. It has been demonstrated that neither nestin mRNA (Dahlstrand et al., 1995) nor nestin immunoreactivity (Clarke et al., 1994) can be observed in the SGZ. We could not find nestin immunoreactivity in the nonischemic SGZ either, except for the signal of vascular origin. We demonstrated that Msi1 can be visualized in vivo in proliferating neuronal progenitor cells in the SGZ. This finding suggests that Msi1 is useful for examining neurogenesis in the SGZ. In the ischemic hippocampus, Msi1-positive cells can be divided into two groups. One group is both nestin- and GFAP-positive reactive astrocytes, and the other is both nestin- and GFAP-negative progenitor cells. In fact, we recently demonstrated the response of neuronal progenitor cells after transient forebrain ischemia by using anti-Msi1 antibody (Yagita et al., 2001; Takasawa et al., 2002). Recently, Seri et al. (2001) demonstrated that BrdU-labeled cells expressed GFAP in the SGZ 2 hr after labeling, but in the majority of them expression of GFAP was abolished 24 hr after labeling. The authors discussed GFAP-negative precursors (named "type D cells") generated from GFAP-positive astrocytes as a primary precursor. In the present study, we showed that cluster-forming cells in the SGZ expressed Msi1 but not GFAP. These cells could correspond to the "type D cells." It seemed that cluster-forming cells, which were labeled with BrdU, were also type D cells, because we observed them an the next day after BrdU injection. It could be possible to observe the in vivo response of neuronal progenitor cells after stimulation by direct identification of type D cells using Msi1. Many researchers are interested in neurogenesis in the SGZ, because this phenomenon could potentially be involved not only in self-repair (Gould and Tanapat, 1997; Liu et al., 1998; Takagi et al., 1999; Lowenstein and Parent, 1999; Kee et al., 2001; Jin et al., 2001; Yoshimura et al., 2001; Yagita et al., 2001) but also in the neuronal plasticity and other hippocampal functions under normal conditions (Kempermann et al., 1997; Gould et al., 1999; van Praag et al., 1999). Differential expression of Msi1 and nestin in neural progenitor cells of the SGZ and SVZ may suggest that we need different strategies for enhancing neurogenesis in these two regions in ischemic stroke. Visualization of neuronal progenitor cells or precursor cells by using anti-Msi1 antibody will help in studies concerning adult neurogenesis in the SGZ.

ACKNOWLEDGMENTS

The authors thank Ms. R. Morimoto and S. Imoto for secretarial assistance. We are also grateful to Dr. Arturo Alvarez-Buylla for critical consultation on this paper. The present study was supported in part by a grant-in-aid from the Ministry of Education, Science and Culture and in part by a Grant-in-aid for Scientific Research (B) and (C), Japan.

REFERENCES

Altman J, Das GD. 1965. Autoradiographic and histological evidence of postnatal hippocampal neurogenesis in rats. J Comp Neurol 124:319–335.

Altman J, Das GD. 1967. Postnatal neurogenesis in the guinea-pig. Nature 214:1098–1101.

Clarke SR, Shetty AK, Bradley JL, Turner DA. 1994. Reactive astrocytes express the embryonic intermediate neurofilament nestin. NeuroReport 5:1885–1888.

Dahlstrand J, Lardelli M, Lendahl U. 1995. Nestin mRNA expression correlates with the central nervous system progenitor cell state in many, but not all, regions of developing central nervous system. Dev Brain Res 84:109–129.

Doetsch F, Caille I, Lim DA, Garcia-Verdugo JM, Alvarez-Buylla A. 1999. Subventricular zone astrocytes are neural stem cells in the adult mammalian brain. Cell 97:703–716.

Duggal N, Schmidt-Kastner R, Hakim AM. 1997. Nestin expression in reactive astrocytes following focal cerebral ischemia in rats. Brain Res 768:1–9.

Eriksson PS, Perfilieva E, Bjork-Eriksson T, Alborn A, Nordborg C, Peterson DA, Gage FH. 1998. Neurogenesis in the adult human hippocampus. Nat Med 4:1313–1317.

Fox GB, Kjoller C, Murphy KJ, Regan CM. 2001. The modulations of NCAM polysialylation state that follow transient global ischemia are brief on neurons but enduring on glia. J Neuropathol Exp Neurol 60:132–140.

Gould E, Tanapat P. 1997. Lesion-induced proliferation of neuronal progenitors in the dentate gyrus of the adult rat. Neuroscience 80:427–436.

Gould E, Tanapat P, McEwen BS, Flugge G, Fuchs E. 1998. Proliferation of granule cell precursors in the dentate gyrus of adult monkeys is diminished by stress. Proc Natl Acad Sci USA 95:3168–3171.

Gould E, Beylin A, Tanapat P, Reeves A, Shors TJ. 1999. Learning enhances adult neurogenesis in the hippocampal formation. Nat Neurosci 2:260–265.

Hockfield S, McKay RD. 1985. Identification of major cell classes in the developing mammalian nervous system. J Neurosci 5:3310–3328.

Imai T, Tokunaga A, Yoshida T, Hashimoto M, Mikoshiba K, Weinmaster G, Nakafuku M, Okano H. 2001. The neural RNA-binding protein musashi1 translationally regulates mammalian numb gene expression by interacting with its mRNA. Mol Cell Biol 21:3888–3900.

Jin K, Minami M, Lan JQ, Mao XO, Batteur S, Simon RP, Greenberg DA. 2001. Neurogenesis in dentate subgranular zone and rostral subventricular zone after focal cerebral ischemia in the rat. Proc Natl Acad Sci USA 98:4710–4715.

Johansson CB, Momma S, Clarke DL, Risling M, Lendahl U, Frisen J. 1999. Identification of a neural stem cell in the adult mammalian central nervous system. Cell 96:25–34.

Kaneko Y, Sakakibara S, Imai T, Suzuki A, Nakamura Y, Sawamoto K, Ogawa Y, Toyama Y, Miyata T, Okano H. 2000. Musashi1: an evolutionally conserved marker for CNS progenitor cells including neural stem cells. Dev Neurosci 22:139–153.

Kaya SS, Mahmood A, Li Y, Yavuz E, Chopp M. 1999. Expression of nestin after traumatic brain injury in rat brain. Brain Res 840:153–157.

Kee NJ, Preston E Woitowicz JM. 2001. Enhanced neurogenesis after transient global ischemia in the dentate gyrus of the rat. Exp Brain Res 136:313–320.

Kempermann G, Kuhn HG, Gage FH. 1997. More hippocampal neurons in adult mice living in an enriched environment. Nature 386:493–495.

Kirschenbaum B, Doetsch F, Lois C, Alvarez-Buylla A. 1999. Adult subventricular zone neuronal precursors continue to proliferate and migrate in the absence of the olfactory bulb. J Neurosci 19:2171–2180.

Leavitt BR, Hemit-Grant CS, Macklis JD. 1999. Mature astrocytes transform into transitional radial glia within adult mouse neocortex that supports directed migration of transplanted immature neurons. Exp Neurol 157:43–57.

Lendahl U, Zimmermann LB, McKay RDG. 1990. CNS stem cells express a new class of intermediate filament protein. Cell 60:585–595.

Li Y, Chopp M. 1999. Temporal profile of nestin expression after focal cerebral ischemia in adult rat. Brain Res 838:1–10.

Lin RCS, Matesic DF, Marvin M, McKay RDG, Brustle O. 1995. Reexpression of the intermediate filament nestin in reactive astrocytes. Neurobiol Dis 2:79–85.

Liu J, Solway K, Messing RO, Sharp FR. 1998. Increased neurogenesis in the dentate gyrus after transient global ischemia in gerbils. J Neurosci 18:7768–7778.

Lois C, Alvarez-Buylla A. 1994. Long-distance neuronal migration in the adult mammalian brain. Science 264:1145–1148.

Lois C, Garcia-Verdugo JM, Alvarez-Buylla A. 1996. Chain migration of neuronal precursors. Science 271:978–981.

Lowenstein DH, Parent JM. 1999. Brain, heal thyself. Science 283:1126–1127.

Nakamura M, Okano H, Blendy JA Montell C. 1994. Musashi, a neural RNA-binding protein required for drosophila adult external sensory organ development. Neuron 13:67–81.

Parent JM, Yu TW, Leibowitz RT, Geschwind DH, Sloviter RS, Lowenstein DH. 1997. Dentate granule cell neurogenesis is increased by seizures and contributes to aberrant network reorganization in the adult rat hippocampus. J Neurosci 17:3727–3738.

Pincus DW, Keyoung HM, Harrison-Restelli C, Goodman RR, Fraser RAR, Edgar M, Sakakibara S, Okano H, Nedergaard M Goldman SA. 1998. Fibroblast growth factor-2/brain-derived neurotrophic factor-associated maturation of new neurons generated from adult human subependymal cells. Ann Neurol 43:576–585.

Reynolds BA, Weiss S. 1992. Generation of neurons and astrocytes from isolated cells of the adult mammalian central nervous system. Science 255:1707–1710.

Sakakibara S, Okano H. 1997. Expression of neural RNA-binding proteins in the postnatal CNS: implications of their roles in neuronal and glial cell development. J Neurosci 17:8300–8312.

Sakakibara S, Imai T, Hamaguchi K, Okabe M, Aruga J, Nakajima K, Yasutomi D, Nagata T, Kurihara Y, Uesugi S, Miyata T, Ogawa M, Mikoshiba K Okano H. 1996. Mouse-musashi-1, a neural RNA-binding protein highly enriched in the mammalian CNS stem cell. Dev Biol 176:230–242.

Seki T, Arai Y. 1993. Highly polysialylated neural cell adhesion molecule (NCAM-H) is expressed by newly generated granule cells in the dentate gyrus of the adult rat. J Neurosci 13:2351–2358.

Seri B, Garcia-Verdugo JM, McEwen BS, Alvarez-Buylla A. 2001. Astrocytes give rise to new neurons in the adult mammalian hippocampus. J Neurosci 21:7153–7160.

Styren SD, Lagenaur CF, Miller PD, Dekosky ST. 1994. Rapid expression and transport of embryonic N-CAM in dentate gyrus following entorhinal cortex lesion: Ultrastructural analysis. J Comp Neurol 349:486–492.

Takagi Y, Nozaki K, Takahashi J, Yodoi J, Ishikawa M, Hashimoto N. 1999. Proliferation of neuronal precursor cells in the dentate gyrus is accelerated after transient forebrain ischemia in mice. Brain Res 831:283–287.

Takasawa K, Kitagawa K, Yagita Y, Sasaki T, Tanaka S, Matsushita K, Ohtsuki T, Miyata T, Okano H, Hori M, Matsumoto M. 2002. Increased proliferation of neural progenitor cells but reduced survival of newborn cells in the contralateral hippocampus after focal cerebral ischemia in rats. J Cereb Blood Flow Metab 22:299–307.

van Praag H, Kempermann G, Gage FH. 1999. Running increases cell proliferation and neurogenesis in the adult mouse dentate gyrus. Nat Neurosci 2:266–270.

Weiss S, Reynolds B, Vescovi A, Morshead C, Craig CG, van der Kooy D. 1996. Is there a neural stem cell in the mammalian forebrain? Trends Neurosci 19:387–393.

Yagita Y, Kitagawa K, Ohtsuki T, Takasawa K, Miyata T, Okano H, Hori M, Matsumoto M. 2001. Neurogenesis by progenitor cells in the ischemic adult rat hippocampus. Stroke 32:1890–1896.

Yoshimura S, Takagi Y, Harada J, Teramoto T, Thomas SS, Waeber C, Bakowska JC, Breakefield XO, Moskowitz MA. 2001. FGF-2 regulation of neurogenesis in adult hippocampus after brain injury. Proc Natl Acad Sci USA 98:5874–5879.

ELSEVIER

Ultrasound in Med. & Biol., Vol. 28, No. 10, pp. 1231–1238, 2002

0301-5629/02/$–see front matter

PII: S0301-5629(02)00578-1

● *Review Article*

THE CAROTID ARTERY AS A NONINVASIVE WINDOW FOR CARDIOVASCULAR RISK IN APPARENTLY HEALTHY INDIVIDUALS

YOJI NAGAI,*† MASAYASU MATSUMOTO* and E. JEFFREY METTER†

*Department of Internal Medicine and Therapeutics, Osaka University Graduate School of Medicine, Osaka, Japan; and †Laboratory of Clinical Investigation, National Institute on Aging, National Institutes of Health, Baltimore, MD, USA

(*Received* 25 *February* 2002; *in final form* 5 *July* 2002)

Abstract—Cardiovascular diseases are the leading cause of death and disability in industrialized countries. Because the etiologies are related to alteration of arterial wall properties, the noninvasive evaluation could help the presymptomatic diagnosis and potentially the prevention of future events. Ultrasound (US) is currently the only modality to image the arterial wall in real-time with sufficient resolution to allow for observation of its morphological, hemodynamic and elastic properties. Increased wall thickness and atheromatous plaques of carotid arteries are associated with cardiovascular risk factors and diseases. Also, carotid Doppler waveforms and wall elasticity may have associations with arterial health. Although evaluation of these arterial properties are currently limited to the research laboratories, most of such properties can be evaluated in the standard setting of carotid ultrasonography. This article reviews "potential" utilities of carotid US evaluation for cardiovascular risk assessment in apparently healthy individuals. (E-mail: nagaiy@medone.med.osaka-u.ac.jp) © **2002 World Federation for Ultrasound in Medicine & Biology.**

Key Words: **Carotid arteries, Atherosclerosis, Arterial elasticity, Ultrasound, Cardiovascular diseases.**

INTRODUCTION

Cardiovascular diseases are the leading cause of death and disability in industrialized countries; their etiologies are related to arterial wall properties changing with age and atherosclerotic risk factors. Thus, evaluation of the wall properties could help the presymptomatic diagnosis and potentially the prevention of future events.

Ultrasound (US) is a noninvasive diagnostic tool commonly used in the clinic. Moreover, it is currently the only modality to image arterial walls in real-time with sufficient resolution to allow for observation of morphological, hemodynamic and elastic properties. In part because of the established utility of US for diagnosing carotid stenosis, such properties are most often evaluated from the carotid arteries. With the use of US, studies have related carotid arterial properties to cardiovascular risk factors and diseases. Because most of such properties can be evaluated in the standard setting of carotid ultrasonography, the evaluation could extend the benefit of examination, potentially facilitating cardiovascular risk assessment in each individual.

Numerous articles exist regarding the diagnosis of carotid stenosis. Also, technical issues relevant to carotid evaluations have been described elsewhere (de Bray et al. 1997; de Bray and Glatt 1995; Reneman et al. 1996; Sidhu and Allan 1997). Nonetheless, there is a paucity of reviews focusing on the added benefits of carotid examination for cardiovascular risk assessment.

This review examines "potential" utilities of carotid US evaluation for cardiovascular risk assessment in apparently healthy individuals.

MORPHOLOGY

Wall thickness

Increased wall thickness as a marker for cardiovascular diseases. High-resolution B-mode imaging allows for the observation of carotid arterial structures, including wall thickness and atheromatous plaques. The common carotid artery (CCA) wall thickness is often evaluated by measuring its intima-media thickness (IMT) (Fig. 1). IMT corresponds to the combined thickness of arterial intimal and medial layers (Pignoli et al. 1986), where

Address correspondence to: Yoji Nagai, M.D., Ph.D., Department of Internal Medicine and Therapeutics, Osaka University Graduate School of Medicine, 2-2 Yamadaoka, Suita, Osaka 565-0871, Japan. E-mail: nagaiy@medone.med.osaka-u.ac.jp

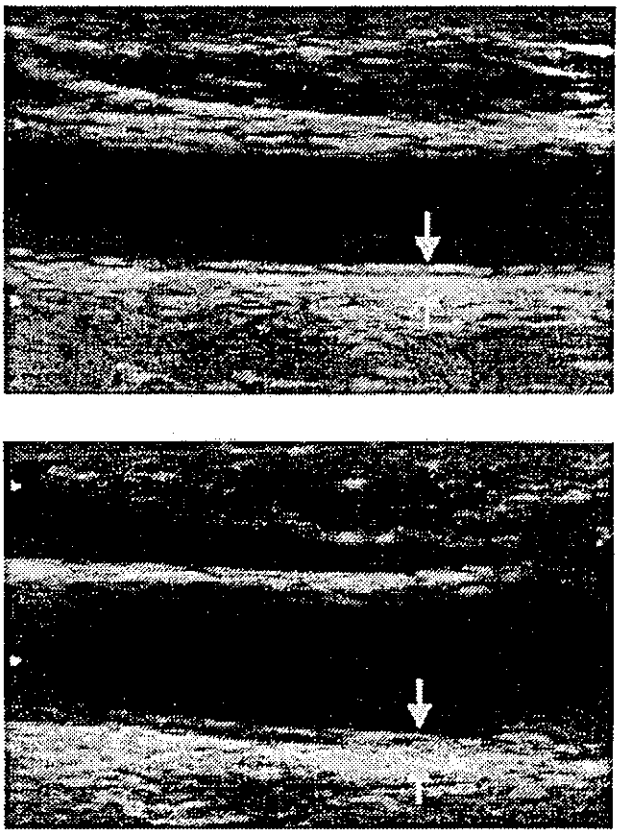

Fig. 1. Intima-media thickness of the common carotid artery; B-mode image of the arterial wall is characterized by two parallel echogenic lines separated by a hypoechogenic space, and the distance between the two lines (arrows) corresponds to IMT. Upper = normal; lower = slightly increased.

atherosclerotic processes proceed. It is often measured from several sites on the far (and near) arterial walls, and the mean and/or maximum are used for cardiovascular risk assessment. However, various methods are currently available with major differences in sampling site, probe frequency and manual vs. computer-assisted image analysis.

Despite such methodological differences, numerous reports have described associations between increased CCA IMT and traditional cardiovascular risk factors, such as age (Howard et al. 1993), hypertension (Zanchetti et al. 1998), diabetes (Kawamori et al. 1992), hyperlipidemia (Poli et al. 1988) and smoking (Howard et al. 1994). Also, increased IMT is linked to relatively new risk factors, including plasma homocysteine (Malinow et al. 1993), angiotensin-converting enzyme activity (Bonithon-Kopp et al. 1994), insulin resistance (Suzuki et al. 1996), cytomegalovirus infection (Nieto et al. 1996), hemostatic factors (Folsom et al. 1993) and cellular adhesion molecules (Rohde et al. 1998). Studies have reported increased IMT in patients with end organ damage, such as left ventricular hypertrophy (Kronmal et al. 1996), cerebral white matter lesions (Bots et al. 1993a) and albuminuria (Agewall et al. 1995), and in those with manifestations of cardiovascular events. Moreover, increased IMT is strongly associated with the presence of atheroma elsewhere in the carotid arteries (Bonithon-Kopp et al. 1996), the coronary arteries (Wofford et al. 1991) and the abdominal aorta (Bots et al. 1993b). Taken together, despite the recent debates as to whether or not IMT represents focal atherosclerosis (Bots et al. 1997b), it is likely to reflect the risk for cardiovascular diseases.

Increased CCA IMT as a risk factor for coronary artery disease (CAD). The association between carotid and coronary atherosclerosis has been well recognized since an autopsy study by Young et al. (1960). Later, Hertzer et al. (1985) demonstrated a high prevalence of CAD in patients with severe carotid atherosclerosis. After the introduction of high-resolution B-mode imaging in the clinic, increased IMT has been associated with angiographic coronary stenosis (Crouse et al. 1995) and overt CAD in the general population (Crouse et al. 1987). Given these findings, the association between increased IMT and manifest CAD appears to be established.

In addition to overt CAD, about 50,000 of 250,000 sudden death victims per year in the USA have no history of heart disease, yet have evidence of advanced coronary atherosclerosis and myocardial scars at autopsy (Warnes and Roberts 1984). This finding suggests the potential impact of asymptomatic CAD as a cause of sudden death. Because asymptomatic CAD frequently progresses to symptomatic CAD (Fleg et al. 1990), early identification could allow for preventive therapies. We have shown increased IMT in asymptomatic volunteers with occult CAD, suggesting the potential utility of IMT measurements for identifying such individuals (Nagai et al. 1998). The utility has been directly supported by the results of large prospective studies. In the Rotterdam Study, each 1-SD (0.15 mm) change in the mean IMT was associated with a 25% increased risk for myocardial infarction in asymptomatic volunteers over 2.7 years, independent of coronary risk factors (Bots et al. 1997a). In the Cardiovascular Health Study, each 1-SD (0.20 mm) change in the maximum IMT was associated with an independent 24% increase in the yearly incidence of myocardial infarction in asymptomatic volunteers (O'Leary et al. 1999). Thus, evaluation of CCA IMT would be useful for the risk stratification of occult and future CAD in apparently healthy individuals.

Increased CCA IMT as a risk factor for cerebrovascular diseases. Because carotid ultrasonography is most often performed for the diagnosis and risk assess-